Inorg. Chem. **2005**, *44*, 7895–7910

Synthesis, Characterization, and X-ray Crystal Structures of Cyclam Derivatives. 8. Thermodynamic and Kinetic Appraisal of Lead(II) Chelation by Octadentate Carbamoyl-Armed Macrocycles[1]

François Cuenot, Michel Meyer, Enrique Espinosa, and Roger Guilard*

Laboratoire d'Ingénierie Moléculaire pour la Séparation et les Applications des Gaz (LIMSAG, UMR 5633 du CNRS), Université de Bourgogne, Faculté des Sciences, 6 boulevard Gabriel, 21100 Dijon, France

Received May 18, 2005

En route toward the development of hybrid organic–inorganic extracting materials incorporating lead-selective chelators and their implementation in water purification processes, the lead(II) binding properties of three *N*-carbamoylmethyl-substituted 1,4,8,11-tetraazacyclotetradecanes (cyclams) have been fully investigated by spectroscopic (IR, UV–vis, MALDI-TOF MS, ^{1}H and ^{13}C NMR), X-ray crystallographic, potentiometric, and kinetic methods. Solution NMR studies revealed that the Pb^{2+} ion is entrapped in a molecular cage constituted by the four macrocyclic nitrogen and four amidic oxygen atoms. Protonation and lead binding constants determined in aqueous solution were shown to be linearly dependent, so that all three derivatives possess a similar affinity at any pH value. Thermodynamic and kinetic parameters revealed the crucial role played by the intramolecular hydrogen bonds also evidenced in the crystal structure of the tetraacetamide derivative **L^1**, which involve the lone pair of each macrocyclic tertiary amine and one amidic hydrogen atom belonging to the appended arm. In contrast to **L^1**, the absence of such intramolecular interactions for *N*-(dimethyl)carbamoylmethyl- and *N*-(diethyl)carbamoylmethyl-substituted cyclams (**L^2** and **L^3**, respectively) accounts for the 2–3 orders of magnitude enhancement of their proton and lead binding affinities. Stopped-flow kinetic measurements enabled unraveling the formation process of the three lead(II) complexes that proceeds in a single rate-limiting step according to the Eigen–Winkler mechanism, while the apparent rate constants were found to increase in the order **L^3** < **L^2** ≪ **L^1** as a consequence of the more acidic character of **L^1**. A common proton-assisted dissociation mechanism has been found for the three lead(II) complexes, which involves the rapid formation of a protonated, six-coordinate intermediate followed by either a unimolecular decomposition or a bimolecular attack of a second hydronium ion.

Introduction

Historically, lead has been one among a handful of readily available metals that shaped human evolution.[2−4] Because lead is not biodegradable it is a persistent contaminant in the environment and remains one of the major public health threats. While two centuries before our era Nicander already recognized the toxicity of cerussite ($PbCO_3$),[2] documentation of numerous cases of poisoning, some with fatal consequences, has led to a resurgence in concern over the past decades. The toxicology of lead is nowadays well documented,[5] although its behavior with respect to biological materials remains yet a field of intense activity. Divalent lead mediates its deleterious effects in part by interfering with zinc and calcium metabolism. It binds to the active site of numerous metalloenzymes and thus inhibits their biological activity.[5] Replacement of the Zn^{2+} center in δ-aminolevulinate dehydratase, the first cytosolic enzyme in the haem

* To whom correspondence should be addressed. Phone: (33) 3 80 39 61 11. Fax: (33) 3 80 39 61 17. E-mail: Roger.Guilard@u-bourgogne.fr.

(1) For the previous paper in this series, see: Meyer, M.; Frémond, L.; Espinosa, E.; Brandès, S.; Vollmer, G. Y.; Guilard, R. *New J. Chem.* **2005**, *29*, 1121−1124.

(2) Grandjean, P. *Environ. Qual. Saf. Suppl.* **1975**, *2*, 6−75.

(3) Wittmers, L. E.; Aufderheide, A.; Rapp, G.; Alich, A. *Acc. Chem. Res.* **2002**, *35*, 669−675.

(4) Claudio, E. S.; Godwin, H. A.; Magyar, J. S. In *Progress in Inorganic Chemistry*; Karlin, K. D., Ed.; Wiley: New York, 2003; Vol. 51, pp 1−144.

(5) Godwin, H. A. *Curr. Opin. Chem. Biol.* **2001**, *5*, 223−227.

10.1021/ic0508019 CCC: $30.25
Published on Web 10/01/2005

biosynthetic pathway, provides a classical example.[6,7] Lead is particularly harmful to children and has uniquely deleterious effects on the brain and central nervous system, increasing the risk for neurocognitive decrements, but long-term exposure is also responsible for kidney injury, anemia, and infertility.[8] In the United States, lead poisoning is still considered to be the most frequent environmentally caused disease as a consequence of an average body burden about 100−1000 times that estimated for prehistoric populations. Blood lead levels higher than 100 μg L^{-1} were estimated for 2.2% of children aged 1−5 years (434 000 children with a 95% confidence interval from 189 000 to 846 000) according to the National Health and Nutrition Examination Survey conducted between 1999 and 2000.[9] Besides absorption of airborne particles through the skin and more efficiently by the lungs due to a larger surface area and a high blood irrigation, lead uptake in humans occurs by ingestion from the gastrointestinal tract of contaminated food and beverages but also dust and old paint chips. The latter source is an important and well-known cause of poisoning for young children, which absorb and eventually accumulate lead more efficiently (50%) than adults (10%). Since most divalent lead compounds are only weakly soluble in vivo, only a limited portion is absorbed, whereas the liposoluble tetraalkyl lead(IV) derivatives easily cross the cellular membranes, and thus most of the absorbed quantity ends up in the brain. Because excretion via the urine and feces is extremely slow, once lead enters the blood the majority (ca. 97%) is rapidly taken up by the erythrocytes, which distribute lead to all soft body tissues and vital organs before being irreversibly deposited in bones (half-life > 20 years), where the Pb^{2+} cations displace the calcium centers in the hydroxyapatite matrix.

To avoid all risks of increasing blood lead levels in infants and protect them against the adverse neurotoxic effects, the World Health Organization (WHO) since 1994 has recommended a maximum uptake of 25 μg per week and kilogram of corporal mass in conjunction with a maximum acceptable concentration in drinking water of 10 μg L^{-1}.[10] Following these guidelines, in 1998 the Council of the European Communities approved the 98/83/CE directive related to the quality of consumption water, requesting the national governments to promulgate bylaws intended to reduce the maximal allowed lead concentration at the consumer's tap from 50 to 25 μg L^{-1} since Dec 2003 and eventually 10 μg L^{-1} in 2013.

Health hazards related to water transport through lead tubing were already recognized as far back as the first century BCE by the roman architect Vitruvius, who recommended in its treaty entitled *De Architectura* conveying water preferentially in terracotta pipes. In the middle of the nineteenth century several reports highlighted the impact of lead-contaminated water consumption on human health.[11] Several cases of acute lead intoxications were reported as, for example, in the Saxon city of Dessau in 1886,[12] which could be jugulated by treatments with limestone and soda ash. As far as regulation is concerned, the total ban of lead pipes imposed in 1878 in the German state of Wurtenberg is probably one of the earliest public-health decisions in that area.[13] On the basis of these historical considerations, it is more than puzzling to realize that the first groundbreaking research programs intended to gain a deeper insight of plumbosolvency and consequently define corrosion-control strategies were launched only in the late 1970s and early 1980s and spurred by the 1978 WHO recommendations that set for the first time a maximal allowed concentration for lead in drinking water.[11,13−16]

Contamination occurs most exclusively through corrosion of services pipes, joints, and solders, although other sources might be responsible for lead levels exceeding in some households 300−400 μg L^{-1}. Dissolution of the mineral coatings mostly composed of hydrocerussite, the basic lead carbonate $Pb_3(CO_3)_2(OH)_2$, deposited at the inner pipe wall or release of scales through erosion are the principal sources for old distribution networks.[16] However, "lead-free" materials and equipment that can contain several percents of lead, such as brass fixtures, tin solders on copper pipes, galvanized steel, and even poly(vinyl chloride) pipes, can significantly contribute to deterioration of the water quality through lead leaching.[17] An estimated 3.3 million lead service lines are located throughout the United States,[18] while a European Community survey carried out in 1995 revealed a much similar, if not worse, situation for West-European countries.[19] For France alone the number of service pipes was estimated to be close to 4 million (38%), corresponding to an approximate total length of 40 000 km, with a much higher occurrence in big cities such as Paris (70%). Furthermore, about the same proportion of home properties (ca. 10 million) were still equipped with internal lead plumbing.[20]

Although replacement of existing lead installations is the ultimate way to ensure that the new 10 μg L^{-1} guideline

(6) Warren, M. J.; Cooper, J. B.; Wood, S. P.; Shoolingin-Jordan, P. M. *Trends Biochem. Sci.* **1998**, *23*, 217−221.
(7) Pauza, N. L.; Cotti, M. J. P.; Godar, L.; de Sancovich, A. M. F.; Sancovich, H. A. *J. Inorg. Biochem.* **2005**, *99*, 409−414.
(8) Chisolm, J. J. In *Diagnosis and Treatment of Lead Poisoning*; Chisolm, J. J., Mahaffey, K. R., Aronson, A. L., Eds.; MSS Information: New York, 1976; pp 158−183.
(9) Second National Report on Human Exposure to Environmental Chemicals; CDC publication 02-0716; U.S. Department of Health and Human Services, Centers for Disease Control and Prevention: Atlanta, 2003.
(10) *Guidelines for drinking water quality*, 2nd ed.; World Health Organization: Geneva, 1994; Vol. 1 (Recommendations).
(11) Schock, M. R.; Wagner, I. In *Internal Corrosion of Water Distribution Systems*; Crnkovich, S., Ed.; AWWA Research Foundation and DVGW−Forschungstelle Cooperative Research Report: Denver, 1985; pp 213−316.
(12) Wolffhügel, G. *Arbeiten am Kaiserlichen Gesundheitsamte II* **1887**, 484.
(13) Kuch, A.; Wagner, I. *Water Res.* **1983**, *17*, 1303−1307.
(14) Schock, M. R. *J.−Am. Water Works Assoc.* **1980**, *72*, 695−704.
(15) Schock, M. R.; Gardels, M. C. *J.−Am. Water Works Assoc.* **1983**, *75*, 87−91.
(16) Schock, M. R. *J.−Am. Water Works Assoc.* **1989**, *81*, 88−100.
(17) Schock, M. R.; Neff, C. H. *J.−Am. Water Works Assoc.* **1988**, *80*, 47−56.
(18) Boyd, G. R.; Tarbet, N. K.; Kirmeyer, G.; Murphy, B. M.; Serpente, R. F.; Zammit, M. *J.−Am. Water Works Assoc.* **2001**, *93*, 74−87.
(19) Jackson, P.; van den Hoven, T.; Wagner, I.; Leroy, P. *The Financial and Economic Implications of a Change of the MAC for Lead*; European Commission Report: 1995.
(20) Leroy, P. *J. Water Supply: Res. Technol., AQUA* **1993**, *42*, 233−238.

Chart 1

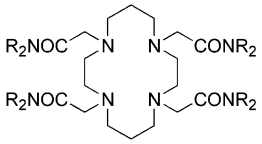

L¹ R = H
L² R = Me
L³ R = Et

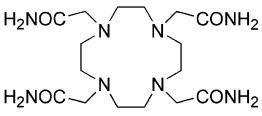

L⁴

value will not be exceeded, retrofitting remains an expensive and long-term task. This prompted us to explore the feasibility of a new concept for a lead-uptake cartridge that could be implemented directly at the consumer's faucet. The principle relies on solid/liquid extraction using a selective macrocyclic lead-sequestering agent covalently attached onto the surface of silica gel.[21] To successfully remove lead in flowing tap water, the ideal chelator should fulfill a number of criteria including the fast formation of stable lead complexes in the typical pH range of drinking water with high selectivity toward the alkaline and earth-alkaline elements usually present at much higher concentrations. To assess the proper ligand design and choice, we thoroughly examined the solution and solid-state behavior of *N*-substituted polyazamacrocycles bearing pendant amide groups with respect to a range of metals commonly present in natural waters.[22−24] As a part of the characterization of tetrafunctionalized cyclam derivatives that might be appropriate models of the sequestering agents incorporated in the solid-phase extracting systems,[25] thermodynamic stabilities of the lead complexes formed with one primary and two tertiary tetraamides (Chart 1) together with their formation and proton-assisted dissociation rates have been evaluated using a range of physical methods including potentiometry, spectroscopy, and stopped-flow absorption spectrophotometry.

Experimental Section

Safety Note. *Although no problems were experienced in handling perchlorate compounds, these salts when combined with organic ligands are potentially explosive and should be manipulated with care and used only in very small quantities.*

Physical and Spectroscopic Measurements. Microanalyses were performed on a Fisons EA 1108 CHNS instrument. The lead content was determined by inductively coupled plasma atomic emission spectrometry (ICP-AES) using a Varian VISTA AX simultaneous spectrometer. MALDI-TOF mass spectra were obtained on a Bruker ProFLEX III spectrometer using dithranol as matrix. The ^{1}H NMR and proton-decoupled ^{13}C NMR spectra were recorded in DMSO-d_6 on a DRX Avance spectrometer (Bruker) operating at 300 MHz. Chemical shifts are expressed in parts per million relative to the residual solvent peak.[26] Infrared absorption spectra were measured as KBr pellets on a IFS 66v (Bruker) Fourier transform spectrophotometer from 4000 to 400 cm^{-1} at 2 cm^{-1} resolution. Electronic absorption spectra were collected with a uniform data point interval of 1 nm on a Cary 50 (Varian) spectrophotometer equipped with a thermostated cell holder connected to a RE106 (Lauda) water circulator. The optical path length of the quartz cell (Hellma) was 1 cm.

Preparation of Compounds. Unless otherwise noted, all chemicals and starting materials were obtained commercially and used without further purification. Cyclam (1,4,8,11-tetraazacyclotetradecane) was synthesized following the procedure of Barefield[27] modified by Guilard et al.,[28] while **L¹**, **L²**, and **L³** were prepared according to previously patented methods.[25]

[Pb(L¹)](ClO₄)₂·3H₂O. Pb(ClO$_4$)$_2$·3H$_2$O (460 mg, 1 mmol) and **L¹** (429 mg, 1 mmol) were dissolved in hot double-deionized water (18.2 MΩ cm). The resulting clear mixture (15 mL) was magnetically stirred at 75−80 °C for 30 min. Slow evaporation at room temperature afforded white crystals, which were isolated and dried in vacuo. Yield: 765 mg, 86%. (+) MALDI-TOF MS: m/z = 429.5 [**L¹** + H]$^+$, 635.4 [Pb(**L¹**) − H]$^+$, 735 [Pb(**L¹**) + ClO$_4$]$^+$. ^{1}H NMR (300 MHz, DMSO-d_6, T = 300 K): δ 1.57 (m, 2H, CH$_2$C*H*$_2$CH$_2$), 1.78 (m, 2H, CH$_2$C*H*$_2$CH$_2$), 2.66 (m, 4H, C*H*$_2$CH$_2$CH$_2$), 2.79 (bs, 8H, NC*H*$_2$CH$_2$N), 2.95 (m, 4H, C*H*$_2$CH$_2$CH$_2$), 3.48 (dd, $^2J_{AB}$ = 15.5 Hz, $\delta\nu$ = 23 Hz, 8H, NC*H*$_2$CO), 7.88 (s, 4H, CON*H*$_2$), 8.26 (s, 4H, CON*H*$_2$). ^{13}C NMR (75 MHz, DMSO-d_6, T = 300 K): δ 25.3 (CH$_2$*C*H$_2$CH$_2$), 55.0 (N*C*H$_2$), 59.2 (N*C*H$_2$CO + N*C*H$_2$), 175.7 (s + d, $J^{207}_{Pb-^{13}C}$ = 14 Hz, CH$_2$*C*O). IR (KBr): υ_{max} = 3500 (ν_{OH}), 3363 ($\nu_{NH\ asym}$), 3171 ($\nu_{NH\ sym}$), 2912 (ν_{CH}), 2867 (ν_{CH}), 2837 (ν_{CH}), 1658 ($\nu_{C=O}$), 1451 (δ_{CH_2}), 1139 (ν_3 ClO$_4^-$), 1109 (ν_3 ClO$_4^-$), 1091 (ν_3 ClO$_4^-$), 626 cm^{-1} (ν_4 ClO$_4^-$). UV (H$_2$O): λ_{max} = 274 nm; ϵ = 6850 M^{-1} cm^{-1}. Anal. Calcd (found) for C$_{18}$H$_{36}$N$_8$Cl$_2$O$_{12}$Pb·3H$_2$O: C, 24.33 (24.62); H, 4.76 (5.22); N, 12.61 (12.64); Pb, 23.32 (23.10).

[Pb(L²)](ClO₄)₂·0.5H₂O. Pb(ClO$_4$)$_2$·3H$_2$O (322 mg, 0.7 mmol) and **L²** (378 mg, 0.7 mmol) were dissolved in a hot methanol/water (10:1 v/v) mixture. The resulting clear solution (22 mL) was magnetically stirred with refluxing for 30 min and then concentrated by removing one-half of the solvent. Slow evaporation at room temperature afforded white crystals, which were isolated and dried in vacuo. Yield: 633 mg, 94%. (+) MALDI-TOF MS: m/z = 540.7 [**L²** + H]$^+$, 746.9 [Pb(**L²**) − H]$^+$, 846.4 [Pb(**L²**) + ClO$_4$]$^+$. ^{1}H NMR (300 MHz, DMSO-d_6, T = 300 K): δ 1.52 (m, 2H, CH$_2$C*H*$_2$CH$_2$), 1.79 (m, 2H, CH$_2$C*H*$_2$CH$_2$), 2.79 (m, 16H, C*H*$_2$CH$_2$CH$_2$ + NC*H*$_2$-CH$_2$N), 2.90 (s, 12H, NC*H*$_3$), 3.05 (s, 12H, NC*H*$_3$), 3.81 (dd, $^2J_{AB}$ = 18 Hz, 8H, NC*H*$_2$CO). ^{13}C NMR (75 MHz, DMSO-d_6, T = 300 K): δ 26.1 (CH$_2$*C*H$_2$CH$_2$), 35.6 (N*C*H$_3$), 36.8 (N*C*H$_3$), 55.0 (N*C*H$_2$), 57.9 (N*C*H$_2$CO), 58.9 (N*C*H$_2$), 172.4 (s + d, $J^{207}_{Pb-^{13}C}$ = 18 Hz, CH$_2$*C*O). IR (KBr): υ_{max} = 3426 (b, ν_{OH}), 2940 (b, ν_{CH}), 2915 (b, ν_{CH}), 2840 (b, ν_{CH}), 1609 ($\nu_{C=O}$), 1144 (ν_3 ClO$_4^-$), 1120 (ν_3 ClO$_4^-$), 1089 (ν_3 ClO$_4^-$), 626 cm^{-1} (ν_4 ClO$_4^-$). UV (H$_2$O): λ_{max} = 274 nm; ϵ = 8070 M^{-1} cm^{-1}. Anal. Calcd (found) for

(21) Cuenot, F.; Meyer, M.; Bucaille, A.; Guilard, R. *J. Mol. Liq.* **2005**, *118*, 89−99.
(22) Meyer, M.; Dahaoui-Gindrey, V.; Lecomte, C.; Guilard, R. *Coord. Chem. Rev.* **1998**, *178−180*, 1313−1405.
(23) Espinosa, E.; Meyer, M.; Berard, D.; Guilard, R. *Acta Crystallogr., Sect. C* **2002**, *58*, m119−m121.
(24) Cuenot, F. Ph.D. Thesis, Université de Bourgogne: Dijon, France, 2004.
(25) Guilard, R.; Roux-Fouillet, B.; Lagrange, G.; Meyer, M.; Bucaille, A. T. PCT Application WO 01 46202, 2001.
(26) Gottlieb, H. E.; Kotlyar, V.; Nudelman, A. *J. Org. Chem.* **1997**, *62*, 7512−7515.
(27) Barefield, E. K. *Inorg. Chem.* **1972**, *11*, 2273−2274.
(28) Guilard, R.; Meunier, I.; Jean, C.; Boisselier-Cocolios, B. U.S. Patent 5 434 262, 1995.

Table 1. X-ray Crystallographic Data for $\mathbf{L^1}\cdot 2H_2O$ and $[\mathbf{L^1}H_2](NO_3)_2\cdot 2H_2O$

	$\mathbf{L^1}\cdot 2H_2O$	$[\mathbf{L^1}H_2](NO_3)_2\cdot 2H_2O$
empirical formula	$C_{18}H_{40}N_8O_6$	$C_{18}H_{42}N_{10}O_{12}$
fw	464.58	590.62
space group	$P2_1/n$	$P\bar{1}$
a, Å	10.5939(9)	8.5200(3)
b, Å	5.1252(3)	8.8830(3)
c, Å	22.100(1)	10.6060(4)
α, deg	90	98.904(2)
β, deg	100.365(9)	108.550(2)
γ, deg	90	111.047(2)
V, Å^3	1180.4(1)	676.60(4)
Z	2	1
T, K	173(2)	110(2)
ρ_{calcd}, g cm^{-3}	1.307	1.450
μ(Mo Kα), mm^{-1}	0.099	0.121
R indices [$I > 2\sigma(I)$][a]	$R_1 = 0.0672$; w$R_2 = 0.1809$	$R_1 = 0.0406$; w$R_2 = 0.0939$
R indices (all data)[a]	$R_1 = 0.0872$; w$R_2 = 0.1925$	$R_1 = 0.0587$; w$R_2 = 0.1048$

[a] $R_1 = \Sigma||F_o| - |F_c||/\Sigma|F_o|$, w$R_2 = \{\Sigma[w(F_o^2 - F_c^2)^2]/\Sigma[w(F_o^2)^2]\}^{1/2}$.

$C_{26}H_{52}N_8Cl_2O_{12}Pb\cdot 0.5H_2O$: C, 32.67 (32.77); H, 5.59 (5.76); N, 11.72 (11.70); Pb, 21.68 (21.62).

$[Pb(\mathbf{L^3})](ClO_4)_2$. $Pb(ClO_4)_2\cdot 3H_2O$ (230 mg, 0.5 mmol) and $\mathbf{L^3}$ (326 mg, 0.5 mmol) were dissolved in hot double-deionized water (18.2 MΩ cm). The resulting clear mixture (50 mL) was magnetically stirred at 75−80 °C for 30 min. Slow evaporation at room temperature afforded white crystals, which were isolated and dried in vacuo. Yield: 333 mg, 62%. (+) MALDI-TOF MS: $m/z = 653.0$ $[\mathbf{L^3} + H]^+$, 858.8 $[Pb(\mathbf{L^3}) - H]^+$, 958.7 $[Pb(\mathbf{L^3}) + ClO_4]^+$. ^{1}H NMR (300 MHz, DMSO-d_6, $T = 300$ K): δ 1.05 (t, $^3J = 6.9$ Hz, 12H, NCH_2CH_3), 1.13 (t, $^3J = 6.9$ Hz, 12H, NCH_2CH_3), 1.53 (m, 2H, $CH_2CH_2CH_2$), 1.86 (m, 2H, $CH_2CH_2CH_2$), 2.82 (m, 8H, CH_2CH_2-CH_2 + NCH_2CH_2N), 2.94 (m, 8H, $CH_2CH_2CH_2$ + NCH_2CH_2N), 3.34 (m + s, $^3J = 6.9$ Hz, NCH_2CH_3 + HDO), 3.83 (dd, $^2J_{AB} = 17.4$ Hz, $\delta\nu = 11$ Hz, 8H, NCH_2CO). ^{13}C NMR (75 MHz, DMSO-d_6, $T = 300$ K): δ 12.5 (NCH_2CH_3), 13.9 (NCH_2CH_3), 26.0 ($CH_2CH_2CH_2$), 40.6 (NCH_2CH_3), 41.6 (NCH_2CH_3), 55.1 (NCH_2), 57.6 (NCH_2CO), 59.3 (NCH_2), 171.5 (s + d, $J^{207}_{Pb-^{13}C} = 19$ Hz, CH_2CO). IR (KBr): $\upsilon_{max} = 2973$ (ν_{CH}), 2936 (ν_{CH}), 2870 (b, ν_{CH}), 1474 (δ_{CH_2}), 1608 ($\nu_{C=O}$), 1089 (b, ν_3 ClO_4^-), 624 cm^{-1} (ν_4 ClO_4^-). UV (H_2O): $\lambda_{max} = 274$ nm; $\epsilon = 8400$ M^{-1} cm^{-1}. Anal. Calcd (found) for $C_{34}H_{68}N_8Cl_2O_{12}Pb$: C, 38.56 (39.12); H, 6.47 (6.67); N, 10.58 (10.78); Pb, 19.56 (19.63).

X-ray Crystallographic Data Collection. Selected crystals were mounted with silicon grease on the tip of a glass capillary. Diffraction data were collected on a Nonius KappaCCD diffractometer,[29] equipped with a nitrogen jet stream low-temperature system (Oxford Cryosystems). The X-ray source was graphite-monochromatized Mo Kα radiation ($\lambda = 0.71073$ Å) from a sealed tube. Lattice parameters were obtained by a least-squares fit to the optimized setting angles of the entire set of collected reflections. Intensity data were recorded as φ and ω scans with κ offsets. No significant intensity decay or temperature drift was observed during the data collections. Data reductions were done by using the DENZO software,[30] without applying absorption correction. The structures were solved by direct methods using the SIR97 program.[31] Refinements were carried out by full-matrix least squares on F^2 using the SHELXL97 program[32] and the complete set of reflections. Anisotropic thermal parameters were used for non-hydrogen atoms. Relevant experimental crystal data and refinement details are summarized in Table 1. Molecular drawings were generated with the ORTEP-3 for Windows application.[33]

$\mathbf{L^1}\cdot 2H_2O$. Colorless prismatic single crystals were obtained from an aqueous solution of $\mathbf{L^1}$ by slow evaporation at room temperature. A high-quality specimen of prismatic shape (0.20 × 0.09 × 0.08 mm^3) was selected for the X-ray diffraction experiment carried out at $T = 173(2)$ K. A total of 8845 reflections were collected in full θ range 3.12−26.36° and merged into 2382 independent reflections ($R_{int} = 0.050$). All hydrogen atoms were found in the Fourier synthesis and refined with a global isotropic thermal factor. While the H(−C) and the amidic H(−N) hydrogen atoms were placed at calculated positions using a riding model (C−H = 0.970 Å, N−H = 1.009 Å), those belonging to the cocrystallized water molecules H(−Ow) were constrained to display Ow−H distances of 0.96 Å. One-half of the molecular unit constitutes the asymmetric unit.

$[\mathbf{L^1}H_2](NO_3)_2\cdot 2H_2O$. Colorless prismatic single crystals were obtained at room temperature by slow evaporation from an aqueous solution of $\mathbf{L^1}$ containing HNO_3 (pH ≈ 3). A high-quality specimen of prismatic shape (0.24 × 0.20 × 0.20 mm^3) was selected for the X-ray diffraction experiment carried out at $T = 110(2)$ K. A total number of 5365 reflections were collected in full θ range 2.13−28.75° and merged into 3446 independent reflections ($R_{int} = 0.031$). All hydrogen atoms were located in the Fourier synthesis. Their positional parameters were refined along with a global isotropic thermal factor. One-half of the molecular unit constitutes the asymmetric unit.

Solution Preparations. All solutions were prepared with boiled and argon-saturated double-deionized high-purity water (18.2 MΩ cm) obtained from a Maxima (USF Elga) cartridge system designed for trace analysis. The carbonate-free NaOH solution, prepared from Merck concentrates (Titrisol), was standardized by titrating against oven-dried (120 °C for 2 h) potassium hydrogenphthalate (Aldrich, 99.99%) and stored under an atmosphere of purified argon using Ascarite II (Acros, 20−30 mesh) scrubbers in order to prevent absorption of carbon dioxide. The 0.1 M $HClO_4$ solution was obtained by dilution of analytical-grade acid (Fischer, 70%) and standardized against 0.1 M NaOH using the equipment described below. Equivalent points were calculated by the second-derivative method. The concentration of the standardized solutions corresponded to the average of at least five replicates and was known with a relative precision of less than 0.15%. All ligand stock solutions were prepared by careful weighing using a Precisa 262SMA-FR balance (precision ±0.01 mg). The mother solution (0.0325 M) of $Pb(ClO_4)_2\cdot 3H_2O$ (Across, >99%) was standardized with a 0.100 M Na_2H_2EDTA solution (Titriplex III, Merck) using xylenol orange as indicator.[34] In all experiments the ionic strength was maintained constant at 0.1 M by addition of the appropriate amount of $NaClO_4\cdot H_2O$ (Merck).

Potentiometric Titrations. Acid−base titrations were carried out in a water-jacketed cell connected to a Lauda RE106 water circulator ensuring a constant temperature of 298.2(2) K. Magnetically stirred solutions were maintained under a low-pressure argon stream to exclude CO_2 from the headspace. Titrant aliquots were delivered through a polypropylene line from a calibrated automatic ABU901 (Radiometer-Tacussel) 10 mL piston buret. Volumes were corrected according to a linear calibration function obtained by weighing known quantities of water and taking into account the

(29) *COLLECT, Data Collection Software*; Nonius BV: Delft, The Netherlands, 1998.
(30) Otwinowski, Z.; Minor, W. *Methods Enzymol.* **1997**, *276*, 307−326.
(31) Altomare, A.; Burla, M. C.; Camalli, M.; Cascarano, G. L.; Giacovazzo, C.; Guagliardi, A.; Moliterni, A. G. G.; Polidori, G.; Spagna, R. *J. Appl. Crystallogr.* **1999**, *32*, 115−119.
(32) Sheldrick, G. M. *SHELXL-97, Program for the Refinement of Crystal Structures*; University of Göttingen: Göttingen, Germany, 1997.
(33) Farrugia, L. J. *J. Appl. Crystallogr.* **1997**, *30*, 565.
(34) *Méthodes d'analyses complexométriques avec les Titriplex*; E. Merck: Darmstadt, 1990.

buoyancy effect.[35] A PHM240 (Radiometer-Tacussel) ionometer was used to record at 0.1 mV resolution the electromotive force between a high-alkalinity XG200 (Radiometer-Tacussel) glass-bulb electrode and a XR300 (Radiometer-Tacussel) Ag/AgCl reference electrode which was separated from the bulk of the solution by a sintered glass bridge filled with 0.1 M $NaClO_4$. To avoid precipitation of $KClO_4$ at the liquid junction, the reference compartment was filled with a saturated NaCl solution. Both instruments were controlled by the Windows-based multitasking and interactive high-resolution titration software HRT Acide-Base Titration developed under the TestPoint environment by C. Mustin.[36] Prior to each experiment, the glass electrode was calibrated to read hydronium ion concentrations ($p[H] = -\log [H_3O^+]$) by titrating 4.000 mL of standardized 0.1 M $HClO_4$ diluted in 25 mL of 0.1 M $NaClO_4$ ($pK_w = 13.78(1)$) with 9.010 mL of 0.1 M standardized NaOH in 0.120 mL increments. Calibration data were processed according to the four-parameter extended Nernst equation which takes into account liquid junction potentials.[37,38]

Protonation constants were determined in the p[H] range 1.8−11.5 by titrating about 0.1 mmol of ligand (ca. 4×10^{-3} M) dissolved in 25 mL of supporting electrolyte (0.1 M $NaClO_4$) acidified with 4.000 mL of 0.1 M $HClO_4$. The electrochemical cell was allowed to equilibrate for at least 1 min after each addition of a 0.030 mL increment of 0.1 M NaOH. The collected potential readings were converted into p[H] values with the help of a Microsoft Excel spreadsheet by iterative solving of the four-parameter calibration function.[37,38] For each system, the individual titration curves were analyzed by the weighed nonlinear least-squares procedure implemented in Hyperquad 2000.[39] In the final refinement step the total amounts of titrated ligand and initially added acid were also allowed to vary. The detailed experimental and data processing procedures have been fully described elsewhere.[37,38] The final values are reported as the arithmetic mean of at least three independent measurements together with their standard deviations, which were systematically higher compared to those derived for a single experiment from the full variance/covariance matrix.[40]

Spectrophotometric Titrations. Potentiometric measurements coupled with a spectrophotometric detection were carried out using the same titration cell and electrode calibration procedure as described above. Visible absorption spectra of a ca. 4×10^{-5} M ligand solution containing an equimolar amount of $Pb(ClO_4)_2$ were recorded in situ as a function of p[H] ranging between 3.9 and 9.4 with a Cary 50 Probe (Varian) spectrophotometer equipped with an immersion probe of 1 cm path length made of SUPRASIL 300 quartz (Hellma, ref 661.202).[38] Prior to titration, the reference spectrum of the 0.1 M $NaClO_4$ supporting electrolyte solution was acquired in the 240−340 nm range. The standard deviation of the measured absorbance for the baseline was constant over the entire wavelength region and did not exceed 0.001 absorbance unit. Aliquots of a standardized 0.01 M NaOH solution containing 0.09 M $NaClO_4$ were added manually with the help of a Gilmont micropipet (2 μL resolution). The potential of the calibrated glass electrode was measured with a PHM240 (Radiometer-Tacussel) ionometer. Enough time was allowed after the addition of each base increment in order to reach the equilibrium. The potential-drift criterion was set at $dE/dt < 0.1$ mV min^{-1}. The collection of absorption spectra was repeated with 2 min delays between two consecutive measurements until superimposable spectra were obtained with optical densities not exceeding 0.5 units. For each titration point, the pH-meter readings were stable in less than 2 min, and no more than two spectral recordings were required. The fitting procedure of the experimental data with the Specfit[41−43] and Hyperquad 2000[39] programs has been fully described elsewhere.[38] Species distribution diagrams were computed with the help of the Hyss software.[44]

Kinetic Measurements. Formation and proton-assisted dissociation kinetic studies were performed under pseudo-first-order conditions by using a SF-61 DX2 stopped-flow spectrophotometer from Hi-Tech Scientific. The drive syringes, mixing chamber, and optical cell were thermostated at 298.2(2) K by water circulating from a RE106 (Lauda) constant-temperature bath. Due to the limited solubility of the diperchlorato complexes in water, the total lead concentration was kept below 5×10^{-5} M. Hence, only the ligand concentration could be varied to ensure pseudo-first-order conditions, albeit in a narrow range comprised between 0.2 and 1×10^{-3} M because of the restricted solubility of the macrocycles. During the course of the formation reaction the p[H] was maintained within ±0.02 units by addition of the nonabsorbing and weakly coordinating 2-(*N*-morpholino)ethanesulfonate buffer (MES, $pK_a = 6.27$ at 298 K). To avoid ligand precipitation the buffering substance was only introduced in the lead perchlorate solution at a concentration of 0.05 M (0.025 M in the reaction mixture), the final p[H] being adjusted with perchloric acid. The reactants maintained at this temperature for at least 15 min prior to injection were mixed in less than 1.5 ms in a flow-through optical quartz cell of 1 cm path length. The kinetic traces, recorded at the maximum of the UV absorption band assigned to the lead complexes (274 nm), were averaged out of at least six replicates and then processed on-line with the fitting routine implemented in the Kinet Asyst 2 (Hi-Tech Scientific) software. This program fits up to three exponential functions to the experimental curves by the Marquardt nonlinear least-squares algorithm.[45] The goodness of fit was judged in terms of the statistical parameter χ^2 (in general, values less than 0.1 were obtained) and by visual inspection of the residual plots. The pseudo-first-order rate constants thus derived are included in the Supporting Information. Linear regression and nonlinear least-squares calculations were performed with Origin 6.0 from Microcal.[46] Standard deviations are reported throughout in parentheses as the last significant digit.

Results

X-ray Crystal Structures of $L^1 \cdot 2H_2O$ and $[L^1H_2](NO_3)_2 \cdot 2H_2O$. Single-crystal X-ray structure analysis of the free-base ligand $\mathbf{L^1}$ and its diprotonated form was performed in order to assess the conformational changes undergone by the molecule upon protonation. Figure 1 shows the ORTEP

(35) Battino, R.; Williamson, A. G. *J. Chem. Educ.* **1984**, *61*, 51−52.
(36) Naja, G.; Mustin, C.; Volesky, B.; Berthelin, J. *Water Res.* **2005**, *39*, 579−588.
(37) Frémond, L.; Espinosa, E.; Meyer, M.; Denat, F.; Guilard, R.; Huch, V.; Veith, M. *New J. Chem.* **2000**, *24*, 959−966.
(38) Meyer, M.; Frémond, L.; Tabard, A.; Espinosa, E.; Vollmer, G. Y.; Guilard, R.; Dory, Y. *New J. Chem.* **2005**, *29*, 99−108.
(39) Gans, P.; Sabatini, A.; Vacca, A. *Talanta* **1996**, *43*, 1739−1753.
(40) Raymond, K. N.; McCormick, J. M. *J. Coord. Chem.* **1998**, *46*, 51−57.
(41) Gampp, H.; Maeder, M.; Meyer, C. J.; Zuberbühler, A. D. *Talanta* **1985**, *32*, 95−101.
(42) Gampp, H.; Maeder, M.; Meyer, C. J.; Zuberbühler, A. D. *Talanta* **1985**, *32*, 251−264.
(43) Gampp, H.; Maeder, M.; Meyer, C. J.; Zuberbühler, A. D. *Talanta* **1985**, *32*, 1133−1139.
(44) Alderighi, L.; Gans, P.; Ienco, A.; Peters, D.; Sabatini, A.; Vacca, A. *Coord. Chem. Rev.* **1999**, *184*, 311−318.
(45) Marquardt, D. W. *J. Soc. Ind. Appl. Math.* **1963**, *11*, 431−441.
(46) *Origin 6.0*; Microcal Software Inc.: Northampton, MA.

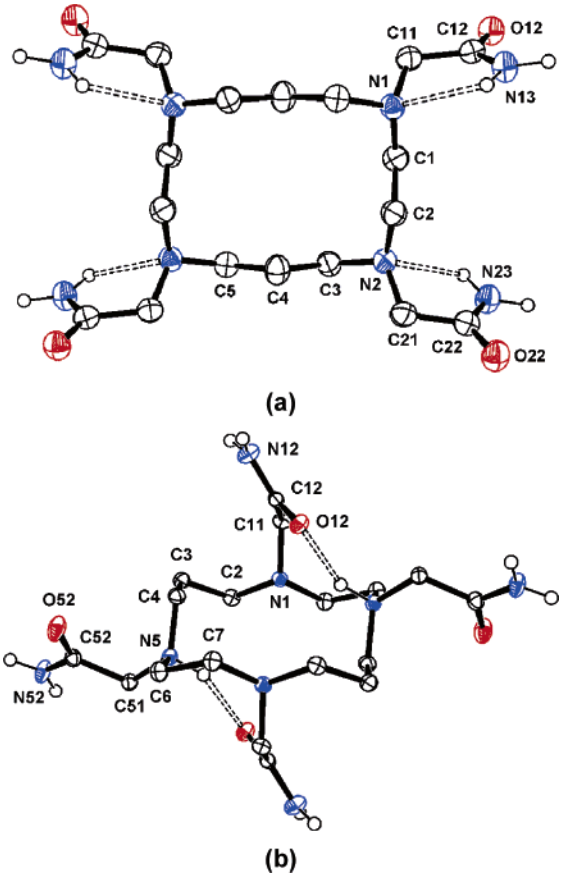

Figure 1. ORTEP diagrams of (a) the free base and (b) the diprotonated form of macrocycle $\mathbf{L^1}$ showing the atom-labeling scheme for one-half of the molecule (symmetry related atoms are labeled according to the same scheme and primed). Thermal ellipsoids are represented at the 50% probability level. All H(−C) hydrogen atoms, counterions, and water molecules have been omitted for clarity.

views of $\mathbf{L^1}$ and $\mathbf{L^1}H_2^{2+}$ together with the numbering scheme. Crystallographic parameters and data collection and refinement information are summarized in Table 1. In both structures the asymmetric unit contains one-half of the molecular unit, the macrocycles being centered on crystallographic inversion centers.

According to the extended Dale's nomenclature that takes into account the exact position of the heteroatoms within the cycle,[22,37] the 14-membered ring of $\mathbf{L^1}$ adopts a fully extended [3,4,3,4]-A conformation. The tertiary amines occupy the four corner positions and thus form a quadrilateral of 3.783 (N1···N2) by 5.116 Å (N1···N2′) with an average C−N−C angle of 114.6(1)°. Starting at τ_1, defined as the N1−C1−C2−N2 torsion angle, the following sequence along the unique ring fragment is observed: $\tau_1-\tau_7$ = 167.3, −71.2, −60.2, 173.5, −168.8, 57.9, and 66.0°. The four pendant *N*-acetamide groups are pointing away from the cavity, one pair belonging to the same propylenediamine subunit is directed above and the other pair below the macrocyclic mean plane. Following the stereochemical description of tetraazamacrocycles introduced by Bosnich et al.,[47] the relative orientation of the four nitrogen substituents can be ascribed to type III. However, each arm is folded toward the cyclam unit as highlighted by the torsional angles C1−N1−C11−C12 (−82°), C5′−N1−C11−C12 (148.4°), C2−N2−C21−C22 (−83.5°), and C3−N2−C21−C22 (146.1°), allowing the nitrogen lone pairs to interact with one terminal amide proton via weak hydrogen bonds (N13···N1 = 2.762 Å, N13−H13b···N1 = 101°; N23···N2 = 2.723 Å, N23−H23b···N2 = 102°). In the crystal packing the cohesion occurs primarily through the intricate intermolecular hydrogen-bond network surrounding each amide oxygen atom as acceptor and terminal NH_2 group as donor (N13···O22 = 2.935 Å, N13−H13a···O22 = 178°; N13···O12 = 2.889 Å, N13−H13b···O12 = 134°; N23···O22 = 2.927 Å, N23−H23b···O22 = 126°; N23···O12 = 2.951 Å, N23−H23a···O12 = 168°). Hence, the twisted conformation of the appended substituents, highlighted by the N1−C11−C12−N13 (−30.5°) and N2−C21−C22−N23 (−28.5°) torsion angles, reflects an equilibrium situation where the spatial arrangement of the arms is mainly imposed by the stronger intermolecular NH···O hydrogen bonds and further stabilized by weaker intramolecular NH···N interactions.

The good quality of the diffraction data for $[\mathbf{L^1}H_2](NO_3)_2\cdot 2H_2O$ enabled the unambiguous identification of two *trans*-located quaternary ammonium sites by visual inspection of the Fourier difference map. Examination of the C(sp^3)−N distances further corroborated the assignment, since the C−N5 bond lengths (1.506(8) Å) are on average significantly longer than those related to the N1 atom (1.468(1) Å), the latter comparing favorably with the mean value found for the free base (1.466(6) Å). As shown in Figure 1b, protonation of the N5 and N5′ tertiary amines induces a pronounced molecular rearrangement, as evidenced by the torsion-angle sequence $\tau_1-\tau_7$ = −55.9, −69.1, −174.7, −68.7, −47.0, 169.8, and −173.0°, with τ_1 = N1−C2−C3−C4. Hence, the cyclam skeleton switches to a quadrangular [3,4,3,4]-C conformation where C3, C6, and the symmetry related atoms are located at the vertexes. It turns out that the directionality of each acetamide group with respect to the N_4 plane is now imposed by the conformational layout of the macrocyclic chain, giving rise to a type IV configuration of the nitrogen atoms.[37] Moreover, the structural changes encountered in $\mathbf{L^1}H_2^{2+}$ also affect the spatial extension of the pendant arms. The amide groups born by the protonated nitrogen atoms are fully extended (N5−C51−C52−N52 = 166.0°) and point away from the cavity center (C4−N5−C51−C52 = −56.9° and C6−N5−C51−C52 = 71.1°). In contrast, both functions attached to N1 and N1′ are folded, one above and the other below the ring (N1−C11−C12−O12 = 38.6°, C2−N1−C11−C12 = 109.4°, and C7′−N1−C11−C12 = −124.4°). Each oxygen atom points toward the adjacent ammonium proton, giving rise to a hydrogen bond (N5···O12′ = 2.784(4) Å, N5−H5···O12′ = 154.9(2)°). The difference in the C12−O12 (1.245(2) Å) and C52−O52 (1.224(2) Å) bond distances translates into a split carbonyl stretching mode in the FTIR spectrum ($\nu_{C=O}$ = 1668 and 1691 cm^{-1}). Furthermore, the H5 proton is also

(47) Bosnich, B.; Poon, C. K.; Tobe, M. L. *Inorg. Chem.* **1965**, *4*, 1102−1108.

involved in a second, albeit much weaker, hydrogen bond with the unprotonated N1′ atom (N5···N1′ = 2.843(2) Å, N5−H5···N1′ = 111.3(1)°). However, the large departure from the ideal value (360°) of the sum of the three angles N5−H5···N1′, N5−H5···O12′, and N1′···H5···O12′ (348.7°) rules out formation of three-center hydrogen bonds,[48] like those found in the diprotonated form of the propionamide analogue of **L1**.[49] The longer arms and the α positioning of the four amines with respect to the corners ([3,4,3,4]-B conformer) account for the slightly different spatial arrangement adopted by the lateral functionalities in both molecules.

Synthesis and Characterization of the Lead(II) Complexes. Although perchlorates are potentially hazardous compounds, spectroscopic arguments prompted us to deliberately choose this anion in the present study because it does not absorb light in the UV range, in contrast to the nitrate salts.[50] Lead(II) complexes of the octadentate *N*-methylcarbamoyl pendant-armed macrocycles were readily obtained by reacting in aqueous media equimolar quantities of **L1**, **L2**, or **L3** with $Pb(ClO_4)_2 \cdot 3H_2O$, followed by crystallization. The MALDI-TOF MS spectra displayed the molecular ion and its perchlorate-adduct peaks with the correct isotope pattern together with the signal assigned to the free ligand. Laser-induced demetalation during the desorption process is a typical behavior for this type of compounds. Elemental analyses were consistent with a $[Pb(L)](ClO_4)_2 \cdot xH_2O$ formulation assuming $x = 3$ (**L1**), 0.5 (**L2**), and 0 (**L3**), in agreement with the presence of broad infrared absorption bands in the 3200−3500 cm^{-1} range for the **L1** and **L2** complexes. Characteristic vibration bands of the cocrystallized perchlorate anions appear in the expected region as a triplet centered around 1110 cm^{-1} (ν_3) and a doublet at 625 cm^{-1} (ν_4), suggesting C_{2v} symmetry in the solid state.[51] Infrared spectroscopy also provided structural evidence for the binding of the amide groups to Pb^{2+} through the oxygen atoms. The FTIR spectra of **L2** and **L3** exhibit a bathochromic shift of ca. 40 cm^{-1} of the carbonyl stretching frequencies as a result of the bond strength weakening upon complexation. Surprisingly, the C=O vibration mode of **L1** is not significantly affected, although the X-ray crystal data obtained for the nitrate complex shows the encapsulation of the lead cation inside the molecular cavity created by both sets of donor atoms, the tertiary amines, and the carbonyl oxygen atoms.[21] However, occurrence in the solid-state structure of $\mathbf{L1} \cdot 2H_2O$ of intermolecular hydrogen-bond interactions involving the amide groups hampers a direct comparison of the free-ligand and metal-complex spectra. It is indeed recognized that hydrogen bonding can shift by several tenths of cm^{-1} to lower energy carbonyl absorption bands.

Table 2. Protonation Constants of **L1**, **L2**, and **L3** and Stability Constants of the Corresponding Lead(II) Complexes[a]

M		L1	L2	L3
H^+	$\log K_{011}$	7.44(2)	8.77(1)	8.85(2)
	$\log K_{012}$	6.38(1)	8.09(1)	8.03(1)
	$\log \beta_{012}$	13.82(2)	16.86(1)	16.88(2)
	$\Delta \log K^b$	1.06	0.68	0.82
Pb^{2+}	$\log \beta_{110}$	8.52(1)	11.30(3)	11.83(3)

[a] $I = 0.1$ M $NaClO_4$; $T = 298.2(2)$ K. [b] $\Delta \log K = \log K_{011} - \log K_{012}$.

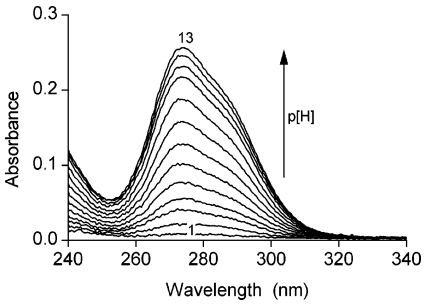

Figure 2. Spectrophotometric titration of **L1** in the presence of Pb^{2+} as a function of p[H]. $[Pb]_{tot} = 3.9 \times 10^{-5}$ M; $[L]_{tot} = 4 \times 10^{-5}$ M; $I = 0.1$ M $NaClO_4$; $T = 298.2(2)$ K; $l = 1$ cm. Spectra 1−13: p[H] = 3.957, 4.312, 4.487, 4.600, 4.719, 4.845, 4.977, 5.135, 5.321, 5.588, 6.143, 8.272, 9.446.

Due to their limited water solubility the solution structure of each complex was characterized in DMSO-d_6 by NMR spectroscopy. ^1H and ^{13}C NMR resonances were assigned using $^1H-^1H$ COSY and $^1H-^{13}C$ HETCOR correlation charts. The spectra are in agreement with the proposed octacoordinated shell structure found in the crystal state for $[Pb(\mathbf{L1})](NO_3)_2$: they exhibit a single set of signals corresponding to one-fourth of the total number of proton or carbon atoms, as expected for dynamic time-averaged C_{2v}-symmetric species. Upon metal binding the four pairs of geminal aliphatic protons become diastereotopic, in agreement with the unidirectional orientation of the four *N*-carbamoylmethyl substituents that differentiates both sides of the cyclam ring. Ligation of the amidic oxygen atoms is supported by a downfield shift (0.85 and 1 ppm, respectively) of both $CONH_2$ resonances as well as by a larger peak separation ($\Delta\delta = 0.22$ ppm for **L1** vs 0.38 for $Pb(\mathbf{L1})^{2+}$). Interestingly, cross-correlation peaks between both terminal *N*-methyl resonances but also between them and the AB spin system appearing at 3.81 ppm assigned to the methylenic arm protons were observed in the COSY map of $Pb(\mathbf{L2})^{2+}$ (Figure S1), supporting four- and even five-bond scalar coupling, respectively, within the rigidified amide chelate rings. It is also worth noting that the ^{13}C NMR carbonyl signal is flanked by two satellite peaks corresponding to the coupling between the carbon nucleus and the 22.6% abundant ^{207}Pb isotope ($I = {}^1/_2$) with $J_{^{207}Pb-^{13}C} \approx 15$ Hz, whereas it appears as a singlet in the free ligand. This observation is a further indication that the encapsulated Pb^{2+} cation is bound to the carbonyl oxygen atoms.

Solution Equilibrium Studies. Overall stability constants β_{mlh} reported hereafter relate to equilibrium 1, where M, L, and H refer to the unhydrolyzed aquametal ion, the ligand, and the hydronium ion, respectively. The associated stoichiometric coefficients are labeled *m*, *l*, and *h*, whereas

(48) Jeffrey, G. A.; Mitra, J. *Acta Crystallogr., Sect. B* **1983**, *39*, 469−480.
(49) Dahaoui-Gindrey, V.; Lecomte, C.; Gros, C.; Mishra, A. K.; Guilard, R. *New J. Chem.* **1995**, *19*, 831−838.
(50) Meyer, M.; Cuenot, F.; Espinosa, E.; Mangayarkarasi, N.; Bucaille, A.; Guilard, R. Unpublished results.
(51) Nakamoto, K. *Infrared and Raman Spectra of Inorganic and Coordination Compounds*; Wiley: New York, 1970.

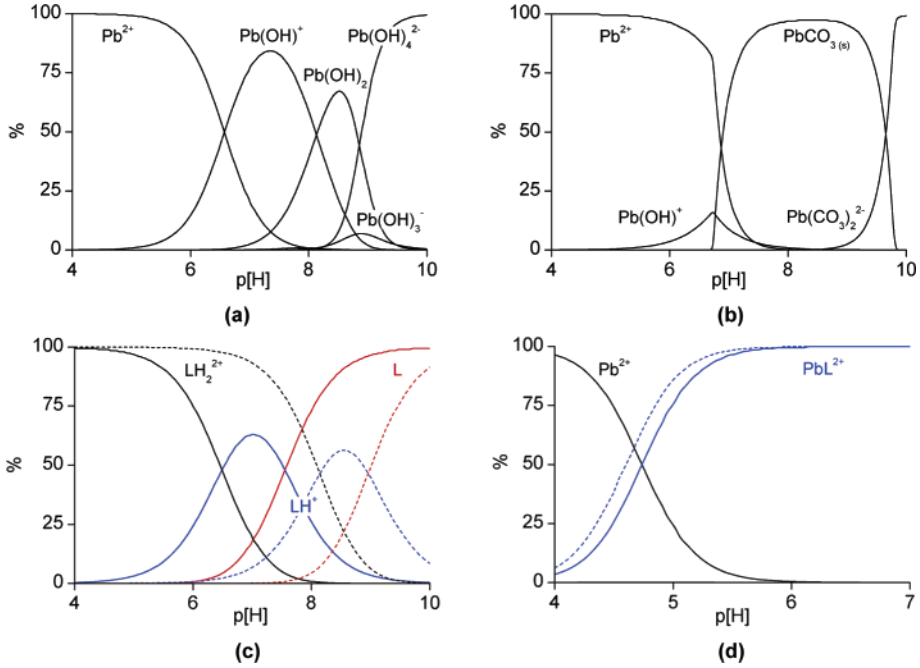

Figure 3. Distribution diagrams of the lead(II) hydroxo and carbonato species ($[Pb]_{tot} = 2 \times 10^{-5}$ M) (a) in anaerobic conditions ($p_{CO_2} = 0$ atm) and (b) under CO_2 atmosphere ($p_{CO_2} = 10^{-3.5}$ atm), (c) of the protonated forms of $\mathbf{L^1}$ (−) and $\mathbf{L^3}$ (--) ($[L]_{tot} = 2 \times 10^{-4}$ M), and (d) of the $Pb^{2+}/\mathbf{L^1}$ (−) and $Pb^{2+}/\mathbf{L^3}$ (--) systems in the absence of CO_2 ($[Pb]_{tot} = 2 \times 10^{-5}$ M; $[L]_{tot} = 2 \times 10^{-4}$ M). Lead hydrolysis and carbonation equilibrium constants were taken from our own critical survey of literature data.[53]

charges have been omitted for clarity. Stepwise protonation constants K_{01i} are defined by the relation $\beta_{01h} = \Pi\, K_{01i}$.

$$mM + lL + hH \rightleftarrows M_mL_lH_h \qquad (1)$$

The acid−base properties in 0.1 M $NaClO_4$ solutions of tetraamines $\mathbf{L^1}$, $\mathbf{L^2}$, and $\mathbf{L^3}$ were investigated at 298.2 K by glass-electrode potentiometry. Analysis of the titration curves acquired between p[H] 1.8 and 11.5 ($p[H] = -\log [H_3O^+]$) indicated only two sequential protonation steps. The corresponding values of the equilibrium constants are collected in Table 2.

The lead(II) uptake by $\mathbf{L^1}$, $\mathbf{L^2}$, and $\mathbf{L^3}$ was monitored at 298.2 K by UV absorption spectrophotometry as a function of p[H] in 0.1 M $NaClO_4$. A typical set of spectra recorded during the titration of equimolar quantities of macrocycle $\mathbf{L^1}$ and Pb^{2+} with sodium hydroxide is depicted in Figure 2. It shows the progressive appearance of the characteristic absorption band of the mononuclear lead(II) complex with a maximum at 274 nm. For each system, singular value decomposition of the complete multiwavelength data array with the program Specfit[41−43] points to the existence of only two spectroscopically distinguishable species (LH_2^{2+} and $Pb(L)^{2+}$). Subsequent nonlinear least-squares refinement of the observed absorbance data confirmed the hypothesized model and afforded best estimates of the complex-formation equilibrium constants β_{110}, which were in excellent agreement with those calculated by fitting the potentiometric data alone with Hyperquad 2000[39] (Table 2). Extinction coefficients calculated by Specfit were, within experimental error, identical to the values obtained after dissolving the pure complex in water ($\epsilon_{max} = 6850$, 8070, and 8400 M^{-1} cm^{-1} at $\lambda_{max} = 274$ nm for $Pb(\mathbf{L^1})^{2+}$, $Pb(\mathbf{L^2})^{2+}$, and $Pb(\mathbf{L^3})^{2+}$, respectively).

The entire set of thermodynamic data reported in Table 2 allowed the computation of the species distribution diagrams shown in Figure 3 as a function of the free proton concentration. According to these curves, the mono- and diprotonated forms of $\mathbf{L^1}$, $\mathbf{L^2}$, or $\mathbf{L^3}$ predominate in the p[H] range 4−7, although a small fraction of the free base is also present at the upper end. Lead(II) exists as a mixture of Pb^{2+} and the soluble hydroxo complex $Pb(OH)^+$ if the solution is protected against CO_2 ingress, while all three complexes are formed at more than 80% above p[H] 5.5.

Formation Kinetics. Taking into account the predominance diagrams depicted in Figure 3, the lead(II) complex formation reaction may be written for each ligand L according to the general formula given by eq 2.

$$Pb(OH)_x^{(2-x)+} + LH_h^{h+} \rightarrow Pb(L)^{2+} + (h - x)\, H^+ \qquad (2)$$

The time course of the complex formation was monitored at 274 nm by single-wavelength stopped-flow spectrophotometry and treated as a pseudo-first-order process by degenerating the reaction order with respect to the ligand. Concentrations after mixing were at least 10 times larger than those of lead(II). Figure 4 shows a typical absorption versus time profile recorded on the millisecond time scale for the insertion of Pb^{2+} (2.015×10^{-5} M) into $\mathbf{L^1}$ present in 30-fold excess (5.98×10^{-4} M). Under such conditions the reaction proceeds to completion in a single rate-limiting step with no more initial loss of spectrophotometric amplitude than that expected from the dead time of the employed instrument. For each system the process was found to be of first order with respect to lead(II). Indeed, the recorded signal could be fitted with excellent statistical confidence to a single-exponential function by nonlinear least squares as

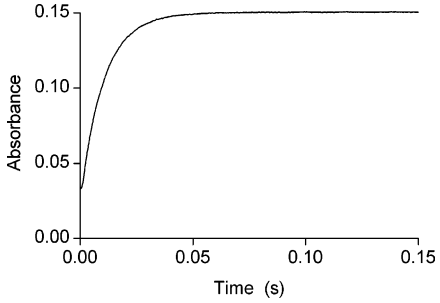

Figure 4. Spectrophotometric signal recorded during the complexation reaction of lead(II) by $\mathbf{L^1}$. $[Pb]_{tot} = 2.015 \times 10^{-5}$ M; $[\mathbf{L^1}]_{tot} = 5.98 \times 10^{-4}$ M; p[H] = 5.48; [MES] = 0.025 M; I = 0.1 M $NaClO_4$; T = 298.2(2) K; λ = 274 nm; l = 1 cm.

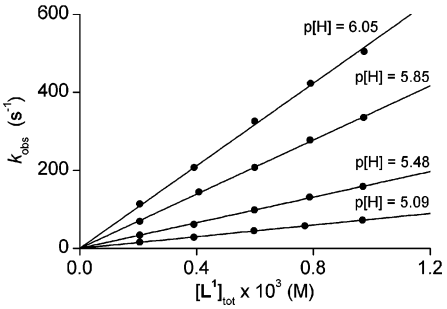

Figure 5. Variation of the pseudo-first-order rate constant k_{obs} with the analytical concentration of $\mathbf{L^1}$ at different p[H] values. $[Pb]_{tot} = 2.015 \times 10^{-5}$ M; [MES] = 0.025 M; I = 0.1 M $NaClO_4$; T = 298.2(2) K.

Table 3. Formation (k_f) and Dissociation (k_d) Rate Constants of Lead(II) Complexes[a]

$\mathbf{L^1}$			$\mathbf{L^2}$			$\mathbf{L^3}$		
p[H]	$k_f \times 10^{-3}$ (M^{-1} s^{-1})	k_d (s^{-1})	p[H]	$k_f \times 10^{-3}$ (M^{-1} s^{-1})	k_d (s^{-1})	p[H]	$k_f \times 10^{-3}$ (M^{-1} s^{-1})	k_d (s^{-1})
4.29	8.8(1)	4.60(4)	5.08	9.2(1)	0.31(6)	5.09	9.3(1)	0
4.45	13.3(1)	3.40(8)	5.40	19.8(1)	0	5.40	18.1(2)	0
4.69	24.5(3)	1.4(3)	5.71	40.6(1)	0	5.71	37.9(1)	0
4.88	42.0(3)	1.1(2)	5.93	67.5(2)	0	5.95	61.0(2)	0
5.09	74.6(3)	0	6.14	112.1(2)	0	6.14	98.5(3)	0
5.48	164(1)	0	6.37	188.0(3)	0	6.39	167.8(7)	0
5.85	347(2)	0	6.63	336.9(4)	0	6.64	294.2(6)	0
6.05	529(5)	0	6.79	452(1)	0	6.78	402(3)	0
			6.98	543(1)	0	6.96	589(1)	0

[a] $[Pb]_{tot} = 2.015 \times 10^{-5}$ M; [MES] = 0.025 M; I = 0.1 M $NaClO_4$; T = 298.2(2) K.

shown in Figure 4. The apparent formation rate constants (k_{obs}) are tabulated in the Supporting Information.

The linear variation of the pseudo-first-order rate constants (k_{obs}) with the analytical concentration of the entering ligand at different p[H] values is graphically displayed in Figure 5 (the raw data may be found in the Supporting Information). At each p[H] the data were fitted to eq 3 by linear regression, supporting the apparent rate law given by eq 4. The values of the second-order k_f and first-order k_d rate constants thus determined are listed in Table 3. The statistical significance of the intercept was evaluated at the 95% probability level by the Student t test.[46,52] When k_d values were negative or

(52) Commissariat à l'Energie Atomique. *Statistique appliquée à l'exploitation des mesures*; Masson: Paris, 1978; Vols. 1−3.

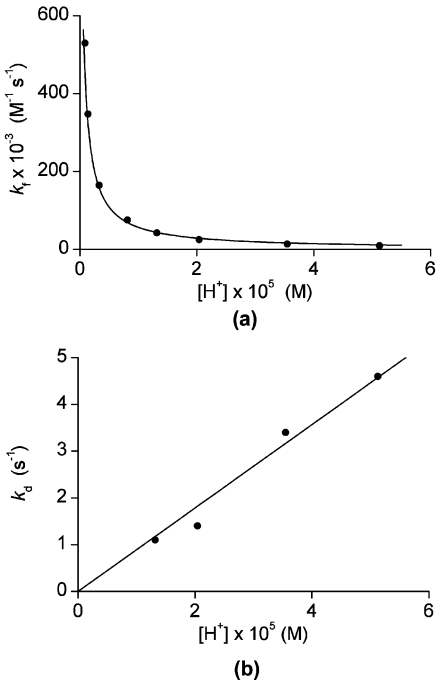

Figure 6. Variations of the rate constants (a) k_f and (b) k_d for $Pb(\mathbf{L^1})^{2+}$ as a function of the proton concentration. [MES] = 0.025 M; I = 0.1 M $NaClO_4$; T = 298.2(2) K.

not significantly different from zero, the experimental data were reprocessed and adjusted to a line passing through the origin.

$$k_{obs} = k_f[L]_{tot} + k_d \quad (3)$$

$$v = \frac{d[Pb(L)^{2+}]}{dt} = k_{obs}[Pb]_{tot} \quad (4)$$

For each investigated system the values of the second-order rate constants k_f gathered in Table 3 are strongly p[H] dependent. Excluding the data points collected near neutrality where a slight deviation occurs, the variation of the k_f values as a function of $[H^+]$ on a bilogarithmic scale affords a straight line with a negative unitary slope supporting an apparent reaction order of −1 with respect to the proton concentration. This general trend, which corresponds to a slowing of the reaction with increasing acid concentration, suggests that different protonated states of one or both reactants, each of them having its own reactivity, are involved in complex formation (Figure 6a). According to the metal and ligand speciation diagrams displayed in Figure 3, the global mechanism is outlined in Scheme 1.

The corresponding rate law derived from Scheme 1 is given by eq 5.

$$v = (k_1[L] + k_3[LH^+] + k_5[LH_2^{2+}])[Pb^{2+}] + (k_2[L] + k_4[LH^+] + k_6[LH_2^{2+}])[Pb(OH)^+] - (k_{-1} + k_{-2}[OH^-] + k_{-3}[H^+] + k_{-4} + k_{-5}[H^+]^2 + k_{-6}[H^+])[Pb(L)^{2+}] \quad (5)$$

According to the mass balance equations, the total ligand concentration can be approximated by eq 6 as a consequence of the pseudo-first-order conditions, while the total lead

Scheme 1

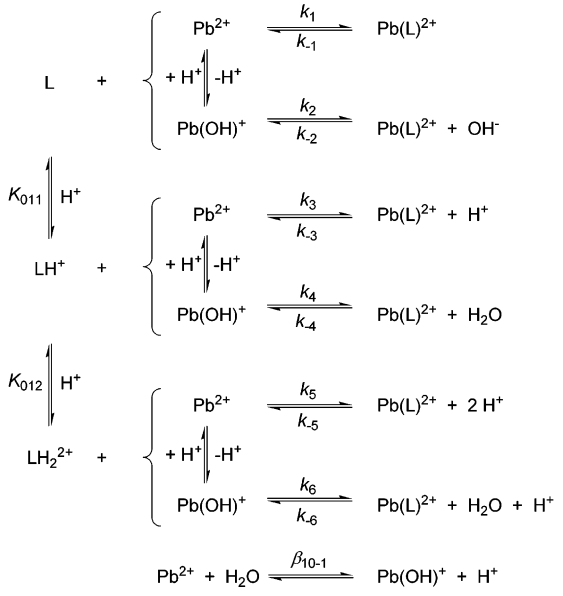

concentration is expressed by eq 7, where β_{011}, β_{012}, and β_{10-1} stand for the first and second cumulative protonation constant of the ligand and for the first hydrolysis constant of Pb^{2+} ($10^{-7.32}$ for $I = 0.1$ $NaClO_4$, $T = 298$ K),[53] respectively.

$$[L]_{tot} = [L] + [LH^+] + [LH_2{}^{2+}] + [Pb(L)^{2+}] \approx [L](1 + \beta_{011}[H^+] + \beta_{012}[H^+]^2)$$

$$[L] = \frac{[L]_{tot}}{(1 + \beta_{011}[H^+] + \beta_{012}[H^+]^2)} \quad (6)$$

$$[Pb^{2+}]_{tot} = [Pb^{2+}] + [Pb(OH)^+] + [Pb(L)^{2+}] = [Pb^{2+}]\left(\frac{[H^+] + \beta_{10-1}}{[H^+]}\right) + [Pb(L)^{2+}]$$

$$[Pb^{2+}] = ([Pb^{2+}]_{tot} - [Pb(L)^{2+}])\left(\frac{[H^+]}{[H^+] + \beta_{10-1}}\right) \quad (7)$$

Substituting the concentrations given by eqs 6 and 7 into eq 5, the rate law rewrites as eq 8, k and $\bar{k}$ being defined by eqs 9 and 10, respectively.

$$v = \frac{d[Pb(L)^{2+}]}{dt} = k[L]_{tot}[Pb]_{tot} - (k[L]_{tot} + \bar{k})[Pb(L)^{2+}] \quad (8)$$

$$k = \{k_2\beta_{10-1} + (k_1 + k_4\beta_{011}\beta_{10-1})[H^+] + (k_3\beta_{011} + k_6\beta_{012}\beta_{10-1})[H^+]^2 + k_5\beta_{012}[H^+]^3\}/\{(1 + \beta_{011}[H^+] + \beta_{012}[H^+]^2)([H^+] + \beta_{10-1})\} \quad (9)$$

$$\bar{k} = k_{-1} + k_{-4} + \frac{k_{-2}K_w}{[H^+]} + (k_{-3} + k_{-6})[H^+] + k_{-5}[H^+]^2 \quad (10)$$

Integration of the corresponding differential, eq 11, yields eq 12, which is mathematically equivalent to the empirical monoexponential fitting function used to model the experimental time-dependent variation of the absorbance at 274 nm since the $Pb(L)^{2+}$ complex is the only absorbing species at this wavelength. Hence, k_f and k_d (eq 3) are, respectively, identified as k and $\bar{k}$.

$$\frac{d[Pb(L)^{2+}]}{[Pb(L)^{2+}] - [Pb(L)^{2+}]_\infty} = -(k[L]_{tot} + \bar{k})dt \quad (11)$$

$$\frac{[Pb(L)^{2+}] - [Pb(L)^{2+}]_\infty}{[Pb(L)^{2+}]_{t=0} - [Pb(L)^{2+}]_\infty} = \exp\{-(k[L]_{tot} + \bar{k})t\} \quad (12)$$

The formation rate constants (k_i, $i = 1-6$) of eq 9 were treated as adjustable parameters by a weighted nonlinear least-squares procedure. The employed weighing scheme ($\omega_i = (1/k_i^{exp})^2$), which was intended to approximately equalize the contribution to the mean square sum of each data point, intrinsically assumes a constant relative error of k_f values over the entire H^+ concentration range. In our conditions only two of the six second-order rate constants k_i could be adjusted; inclusion of an additional parameter led systematically to divergence. Moreover, we were faced with proton ambiguity since data refinement by two different models yields the same goodness-of-fit criterion χ^2.[46] All the results summarized in Table 4 are consistent with a reaction mechanism involving the unhydrolyzed Pb^{2+} cation and the monoprotonated form of each macrocycle (k_3). Considering this sole pathway in the p[H] region where $LH_2{}^{2+}$ and Pb^{2+} predominate, eq 9 reduces to $k \approx (k_3/K_{012}) \times [H^+]^{-1}$, in agreement with the empirical rate law suggested by the bilogarithmic representation of k_f vs $[H^+]$. The deviations from the straight line for the data points collected at p[H] values close to 7 are equally well explained by considering the reaction of either Pb^{2+} with the deprotonated ligand species L (k_1) or the monohydrolyzed $Pb(OH)^+$ cation with the monoprotonated macrocycle LH^+ (k_4) as the additional pathway. Unfortunately, the appearance of precipitates above p[H] 7 precluded a more detailed investigation of the complexation mechanism in alkaline media.

As far as the reverse reactions are concerned, significant k_d values increasing linearly with the proton concentration were only obtained for $\mathbf{L^1}$ below p[H] 5 (Figure 6b). According to eq 10, the slope of the best-fit line passing through the origin corresponds to the sum $k_{-3} + k_{-6} = 8.9(4) \times 10^4$ M^{-1} s^{-1}. Since the forward rate constant k_6 was inaccessible, it is reasonable to assume also that $k_{-6} \approx 0$. The absence of any significant ordinate at the origin further suggests that $k_{-1} + k_{-4}$ is negligible as well as k_{-2} and k_{-5}, which would lead to a nonlinear dependence of k_d vs $[H^+]$. Conversely, none of the six reverse rate constants k_{-i} could be determined directly for $\mathbf{L^2}$ and $\mathbf{L^3}$ under the experimental conditions used herein. Taking into account the equilibrium constants reported in Table 2, the computed estimates of $k_{-1} = k_1/\beta_{110}$ (3.0×10^{-2}, 1.3×10^{-3}, and 3.4×10^{-4} M^{-1} s^{-1} for $\mathbf{L^1}$, $\mathbf{L^2}$, and $\mathbf{L^3}$, respectively) and $k_{-3} = k_3 \times K_{011}/\beta_{110}$ (1.1×10^5, 2.9×10^4, and 8.2×10^3 M^{-1} s^{-1} for $\mathbf{L^1}$, $\mathbf{L^2}$, and $\mathbf{L^3}$, respectively) are in good accordance with the above-mentioned results.

(53) Cuenot, F.; Meyer, M.; Guilard, R. Unpublished results.

Table 4. Values of Second-Order Formation Rate Constants k_1, k_3, and k_4 Fitted by Nonlinear Least Squares for Various Models[a]

model	k_1 (M^{-1} s^{-1})	k_3 (M^{-1} s^{-1})	k_4 (M^{-1} s^{-1})	χ^2
$Pb^{2+} + \mathbf{L^1}$ and $Pb^{2+} + \mathbf{L^1}H^+$	$10(2) \times 10^6$	$13.6(5) \times 10^5$		0.0083
$Pb^{2+} + \mathbf{L^1}H^+$ and $Pb(OH)^+ + \mathbf{L^1}H^+$		$13.6(5) \times 10^5$	$7(1) \times 10^6$	
$Pb^{2+} + \mathbf{L^2}$ and $Pb^{2+} + \mathbf{L^2}H^+$	$25(3) \times 10^7$	$98(1) \times 10^5$		0.00091
$Pb^{2+} + \mathbf{L^2}H^+$ and $Pb(OH)^+ + \mathbf{L^2}H^+$		$98(1) \times 10^5$	$90(9) \times 10^5$	
$Pb^{2+} + \mathbf{L^3}$ and $Pb^{2+} + \mathbf{L^3}H^+$	$23(2) \times 10^7$	$78(1) \times 10^5$		0.00076
$Pb^{2+} + \mathbf{L^3}H^+$ and $Pb(OH)^+ + \mathbf{L^3}H^+$		$78(1) \times 10^5$	$67(6) \times 10^5$	

[a] [MES] = 0.025 M; I = 0.1 M $NaClO_4$; T = 298.2(2) K.

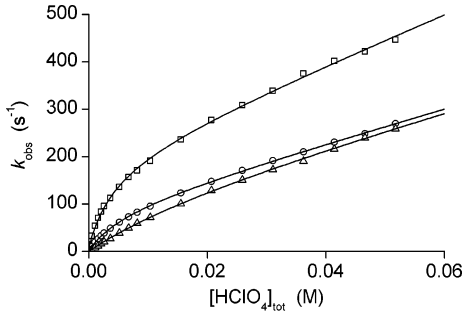

Figure 7. Variation of the pseudo-first-order rate constant k_{obs} for the dissociation of the lead(II) complexes as a function of proton concentration. Solid lines were drawn according to eq 15 and the refined parameters collected in Table 5. (□) $[Pb(\mathbf{L^1})^{2+}]_{tot} = 1.84 \times 10^{-5}$ M; (○) $[Pb(\mathbf{L^2})^{2+}]_{tot} = 1.80 \times 10^{-5}$ M; (△) $[Pb(\mathbf{L^3})^{2+}]_{tot} = 1.13 \times 10^{-5}$ M; I = 0.1 M (H,Na)ClO_4; T = 298.2(2) K.

Dissociation Kinetics. The proton-assisted dissociation processes of the three lead(II) complexes have also been studied by stopped-flow absorption spectrophotometry. The overall reaction writes as eq 13.

$$Pb(L)^{2+} + 2H^+ \rightarrow Pb^{2+} + LH_2^{2+} \qquad (13)$$

Kinetic runs were performed under pseudo-first-order conditions by mixing the lead(II) complex ($1-2 \times 10^{-5}$ M) with perchloric acid in large excess (2×10^{-4} M < $[H^+]_{tot}$ < 5×10^{-2} M). At any acid concentration the reaction was quantitative, as evidenced by the total disappearance of the UV absorption band. Moreover, experimental absorbance data, recorded as a function of time at 274 nm, evidenced no significant amplitude loss during the mixing time and were fitted as a single-exponential decay with excellent confidence. Thus, the proton-assisted demetalation reaction follows first-order kinetics with respect to the complex. The apparent dissociation rate law is expressed by the differential eq 14, where k_{obs} represents the pseudo-first-order dissociation rate constant.

$$v = -\frac{d[Pb(L)^{2+}]}{dt} = k_{obs}[Pb(L)^{2+}] \qquad (14)$$

Plots of k_{obs} versus $[H^+]_{tot}$ for the three complexes (Figure 7; the raw data may be found in the Supporting Information) show a saturation behavior at low acid concentrations ($[H^+]_{tot}$ < 0.02 M) followed by a quasi-linear increase at higher concentrations. Nonlinear least-squares analysis provided an excellent agreement between the data plotted in Figure 7 and the rate expression given by eq 15. Best estimates of the adjusted parameters (K, k_d, k^H_1, and k^H_2) are presented in Table 5.

Table 5. Nonlinear Least-Squares Adjusted Values of k_d, k^H_1, k^H_2, and K for the H^+−Assisted Demetalation Kinetics[a]

	$Pb(\mathbf{L^1})^{2+}$	$Pb(\mathbf{L^2})^{2+}$	$Pb(\mathbf{L^3})^{2+}$
k_d (s^{-1})	9(4)	1.6(9)	0
K (M^{-1})	$2.2(3) \times 10^2$	$1.6(1) \times 10^2$	$0.44(9) \times 10^2$
k^H_1 (s^{-1})	$2.2(1) \times 10^2$	$1.18(5) \times 10^2$	$1.9(3) \times 10^2$
k^H_2 (M^{-1} s^{-1})	$5.2(2) \times 10^3$	$3.56(6) \times 10^3$	$3.4(2) \times 10^3$

[a] I = 0.1 M (H,Na)ClO_4; T = 298.2(2) K.

$$k_{obs} = \frac{k_d + k^H_1 K[H^+]_{tot} + k^H_2 K[H^+]_{tot}^2}{1 + K[H^+]_{tot}} \qquad (15)$$

Discussion

Solution Thermodynamics. In the investigated p[H] range (1.8−11.5) the three tetraamines behave as a moderately strong diprotic base. As a common feature among cyclam derivatives,[54] the tri- and tetraprotonated species do not form in any appreciable amount, even in strongly acidic aqueous solutions, as a consequence of positive charge accumulation. The difference $\Delta\log K = \log K_{011} - \log K_{012}$ directly reflects the electrostatic repulsion energy between the ammonium centers once the statistical factor has been factored out ($\Delta\log K = \log 8/3 \approx 0.43$ for a receptor possessing four identical and independent binding sites).[55] For each macrocycle, the much larger than expected $\Delta\log K$ value experimentally observed (Table 2) reveals strong Coulombic interactions in the diprotonated form, preventing further proton addition.

Data in Table 2 also indicate an increase of the overall basicity when the primary acetamide groups ($\mathbf{L^1}$) are replaced by either *N*,*N*-dimethyl- ($\mathbf{L^2}$) or *N*,*N*-diethyl- ($\mathbf{L^3}$) carbamoylmethyl arms. The 3 orders of magnitude difference between the β_{012} values recorded for primary and tertiary amides can be understood in terms of intramolecular hydrogen-bond formation between the macrocyclic nitrogen and amidic hydrogen atoms of $\mathbf{L^1}$. Involvement of each nitrogen free-electron doublet in a five-membered ring, as observed in the crystal structure, hinders the protonation process and lowers by several orders of magnitude the proton affinity of a tertiary amine in water, as demonstrated by several authors.[56−61] Obviously, such N−H···N interactions

(54) Bencini, A.; Bianchi, A.; Garcia-Espana, E.; Micheloni, M.; Ramirez, J. A. *Coord. Chem. Rev.* **1999**, *188*, 97−156.
(55) Perlmutter-Hayman, B. *Acc. Chem. Res.* **1986**, *19*, 90−96.

cannot occur in $\mathbf{L^2}$ or $\mathbf{L^3}$, so that protonation constants remain typical for tertiary amines bearing electron-withdrawing groups.[62] In comparison, K_{011} and K_{012} values reported for 1,4,8,11-tetramethyl-1,4,8,11-tetraazacyclotetradecane (TMC) are approximately 10 times higher (log K_{011} = 9.39 and log K_{012} = 9.05; I = 0.1 $NaNO_3$; T = 298.2 K).[63]

Since the three macrocycles exhibit different acid−base properties, speciation calculations provide an accurate means to discuss their lead binding affinity.[21] As can be seen in Figure 3d, the efficiencies of the primary and tertiary amides are essentially identical, although the latter species form complexes that are 3 orders of magnitude more stable than the former. Comparison of the β_{110} and β_{012} values found in Table 2 indicates that the higher stability of $Pb(\mathbf{L^2})^{2+}$ and $Pb(\mathbf{L^3})^{2+}$ over $Pb(\mathbf{L^1})^{2+}$ parallels the higher basicity exhibited by the free bases $\mathbf{L^2}$ or $\mathbf{L^3}$. Hence, the lower affinity of $\mathbf{L^1}$ for lead(II) is almost integrally compensated by its more acidic character, leading to a similar lead affinity at any given p[H] value. Besides carboxylic, phosphonic, and phosphinic tetraamino derivatives, our series provides an additional example where the stability of the metal complexes is essentially governed by the ligand's overall basicity.[64]

Formation Kinetics. Our kinetic investigations have evidenced a single rate-limiting step process leading to the fast formation of the lead(II) complexes, although the medium's acidity level exerts a marked influence on the overall reaction rate. This has some important practical consequences if one seeks to implement related amide-substituted cyclam sequestrants in solid/liquid extraction processes.[21] Keeping in mind that the ultimate goal of this study was to provide an appraisal of the kinetic lead-uptake performances of ligands $\mathbf{L^1}$−$\mathbf{L^3}$, only the apparent complexation rate constants (k_{obs}) under precisely defined p[H] conditions and concentrations enable a direct comparison. Hence, each p[H]-dependent curve plotted in Figure 8 has been calculated for a total ligand concentration of 10^{-3} M by combining eqs 9 and 10 with the rate law expression, eq 3. Although it should be stressed that lead speciation in tap water at pH values between 6 and 9 differs noticeably from the actual solution compositions used in this study due to the predominance of soluble $Pb(CO_3)$,[65,66] Figure 8 provides

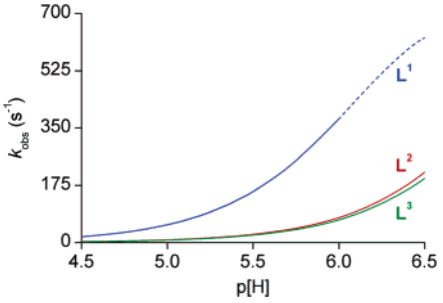

Figure 8. Comparison of the apparent pseudo-first-order formation rate constant k_{obs} calculated for $[L]_{tot} = 10^{-3}$ M as a function of p[H]. I = 0.1 M $NaClO_4$; T = 298.2(2) K. The portion of the dotted line drawn for $\mathbf{L^1}$ shows that the corresponding rate constants become too fast to be measured by a stopped-flow mixing device.

valuable clues as the lead-uptake rate increases in the order $\mathbf{L^3} \approx \mathbf{L^2} \ll \mathbf{L^1}$. The superior kinetic performances evidenced by $\mathbf{L^1}$ over $\mathbf{L^2}$ and $\mathbf{L^3}$ in weakly acidic media are essentially related to its less basic character as shown in Figure 3c, whereas the tertiary amides are essentially present below p[H] 7 in their almost unreactive diprotonated form.

From a mechanistic point of view, the p[H] dependency of the second-order formation rate constants k_f could be satisfactorily rationalized in terms of two parallel paths, although proton ambiguity hampers the definitive assignment. Nevertheless, data in Table 4 show that Pb^{2+} and the monoprotonated macrocycle are the main reacting species (k_3) below p[H] ≈ 5.5, although the LH_2^{2+} form predominates in solution. Close to neutrality an alternative pathway becomes operative but the reaction of Pb^{2+} with L (k_1) is kinetically indistinguishable from that of $Pb(OH)^+$ with LH^+ (k_4). As found for several main-group and transition-metal cations,[67] it might be argued that the monohydrolyzed lead species $Pb(OH)^+$ is more reactive than the aquated Pb^{2+} cation due to labilization of the water molecules in the first solvation shell by the hydroxo ligand, leading to a partial charge transfer to the metal. The anticipated rate-enhancement factor might be on the order of $10-10^4$, whereas the k_4/k_3 ratio does not exceed 5 in the case of $\mathbf{L^1}$ and is even less than unity for the two other ligands (Table 4). Conversely, the refined k_1 values corresponding to the reaction of Pb^{2+} with the free-base ligands are systematically higher by a factor of 7−30 than those found for k_3. This result is fully consistent with the more favorable electrostatic interaction in the early stage of the complexation process when the divalent lead cation reacts with an uncharged rather than a monopositively charged macrocycle (vide infra). Relying on these arguments, participation of $Pb(OH)^+$ in the mechanism depicted in Scheme 1 can be ruled out, thus solving the proton ambiguity.

The kinetic parameters derived in the present work evidence a noticeable influence of rather minor structural changes in the ligands $\mathbf{L^1}$−$\mathbf{L^3}$ on the reaction rate. Considering the second-order rate constants k_3 that mirror the intrinsic reactivity of the monoprotonated macrocycles, the methylated $\mathbf{L^2}H^+$ and ethylated $\mathbf{L^3}H^+$ tetraamides react about 7 times more rapidly with Pb^{2+} than the less crowded acetamide

(56) Serratrice, G.; Mourral, C.; Zeghli, A.; Béguin, C. G.; Baret, P.; Pierre, J. L. *New J. Chem.* **1994**, *18*, 749−758.
(57) Caris, C.; Baret, P.; Pierre, J. L.; Serratrice, G. *Tetrahedron* **1996**, *52*, 4659−4672.
(58) Cohen, S. M.; Meyer, M.; Raymond, K. N. *J. Am. Chem. Soc.* **1998**, *120*, 6277−6286.
(59) Xu, J.; O'Sullivan, B.; Raymond, K. N. *Inorg. Chem.* **2002**, *41*, 6731−6742.
(60) Kotek, J.; Lubal, P.; Hermann, P.; Cisarova, I.; Lukes, I.; Godula, T.; Svobodova, I.; Taborsky, P.; Havel, J. *Chem.−Eur. J.* **2003**, *9*, 233−248.
(61) Wang, Y. M.; Li, C. R.; Huang, Y. C.; Ou, M. H.; Liu, G. C. *Inorg. Chem.* **2005**, *44*, 382−392.
(62) Smith, R. M.; Martell, A. E.; Motekaitis, R. J. *NIST Critically Selected Stability Constants of Metal Complexes Database*, release 6.0; NIST Standard Reference Data No. 46: NIST: Gaithersburg, MD, 2001.
(63) Grzejdziak, A. *Monatsh. Chem.* **1994**, *125*, 107−117.
(64) Lukes, I.; Kotek, J.; Vojtisek, P.; Hermann, P. *Coord. Chem. Rev.* **2001**, *216−217*, 287−312.
(65) Hem, J. D.; Durum, W. H. *J.−Am. Water Works Assoc.* **1973**, *65*, 562−568.
(66) Hem, J. D. *Geochim. Cosmochim. Acta* **1976**, *40*, 599−609.
(67) Lincoln, S. F.; Merbach, A. E. *Adv. Inorg. Chem.* **1995**, *42*, 1−88.

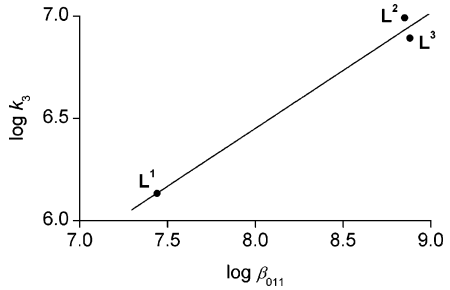

Figure 9. Linear free energy relationship between the second-order rate constants k_3 and the first protonation constants β_{011}. $I = 0.1$ M $NaClO_4$; $T = 298.2(2)$ K.

derivative $\mathbf{L^1}H^+$. The empirical linear free-energy relationship between log k_3 and log β_{011} values displayed in Figure 9 provides a reasonable explanation for this significant effect. The weaker basicity of $\mathbf{L^1}$ compared to its analogues $\mathbf{L^2}$ and $\mathbf{L^3}$ has been ascribed to the formation of intramolecular hydrogen bonds engaging the free electron pair of each tertiary amine and its appended acetamide group in a five-membered ring. Provided such interactions might also occur in the monoprotonated state, the decreased reactivity of $\mathbf{L^1}H^+$ can directly be related to the necessity to break these hydrogen bonds prior to Pb−N bond formation and the concomitant chelate ring closure.[60,68] Finally, increased steric hindrance provided by the *N*-terminal ethyl groups can be put forward to explain the slightly slower formation of $Pb(\mathbf{L^3})^{2+}$ ($k_3 = 7.8(1) \times 10^6$ M^{-1} s^{-1}) with respect to $Pb(\mathbf{L^2})^{2+}$ ($k_3 = 9.8(1) \times 10^6$ M^{-1} s^{-1}).

Moreover, the great sensitivity of the formation rate constant k_3 to structural factors such as the macrocyclic ring size is also evidenced by comparing the data measured for the 14-membered cyclam and 12-membered cyclen tetraacetamide derivatives $\mathbf{L^1}$ and $\mathbf{L^4}$. While the overall reaction mechanism remains the same, enlarging the cyclen framework of $\mathbf{L^4}H^+$ ($k_3 = 1.19(4) \times 10^5$ M^{-1} s^{-1})[24] by two carbon atoms, as found in $\mathbf{L^1}H^+$ ($k_3 = 1.36(5) \times 10^6$ M^{-1} s^{-1}), induces a 10-fold increase of the complexation rate. Since both ligands bear the same chelating side chains, this difference reflects the enhanced rigidity and the higher steric strain exhibited by the smaller macrocycle $\mathbf{L^4}$ as it wraps around the Pb^{2+} cation. Nevertheless, this trend of higher rates when the ring size changes from 12 to 14 atoms suffers from numerous exceptions.[69−71] For instance, no pronounced differences in the kinetic parameters were noticed for the insertion of Ca^{2+}, Zn^{2+}, or Ni^{2+} in the tetraacetate analogues of $\mathbf{L^1}$ and $\mathbf{L^4}$, namely $TETAH^{3-}$ and $DOTAH^{3-}$.[68]

Identification of the actual position of the rate-determining step is one point of interest in discussing the complex formation mechanism with multidentate cyclic chelators.[72] To that end, the experimental second-order rate constants can be compared with the limiting values predicted by the Eigen−Wilkins theory for a dissociative D or I_d mechanism involving unidentate ligands.[73,74] For the reaction scheme outlined in eq 16, the rate constant of the second-order process is controlled by the rate of solvent exchange in the first solvation sphere of the metal cation (k_{ex}) and is expressed by the product $k_{EW} = K_{OS} \times k_{ex}$, assuming a steady-state regime.

$$MS_x + L \overset{K_{OS}}{\rightleftharpoons} \{MS_x\cdots L\} \xrightarrow{k_{ex}} MS_{x-1}L + S \xrightarrow{+L} MS_{x-2}L_2 + S \xrightarrow[\text{steps}]{\text{fast}} ML_x \quad (16)$$

K_{OS} corresponds to the equilibrium constant for the fast formation of an outer-sphere complex. In practice, estimates of K_{OS} are computed with the Fuoss equation.[75] The water-exchange rate constant for Pb^{2+} at 298 K has been measured by Yasunaga and Harada.[76] These authors proposed a value of 7.5×10^9 s^{-1} based on ultrasonic relaxation experiments. Accordingly, the kinetic parameters are expected to be insensitive to the chemical nature of the entering ligand since the key step is the displacement of a water molecule in the first solvation shell. Unfortunately, a detailed discussion of the lead-association mechanism and rates is hampered by the scarcity of kinetic data available in the literature. Formation rates that are pertinent to the following discussion are reviewed in Table 6.

The largest body of information has been collected for polyaminocarboxylic open-chain chelators. Overall, these compounds display the highest reaction rates with intrinsic

Table 6. Intrinsic Formation Constants (k'_f) of Lead(II) Tetraaza-macrocyclic Complexes in Water at 298.2 K[a]

ligand		k'_f (M^{-1} s^{-1})	k'_f/k_{ex} (M^{-1})	I (M)	ref
EDTA	LH^{3-}	6.1×10^{11}	81	0.3	96
HEDTA	LH^{2-}	2.4×10^{11}	32	0.3	96
EDDDA	LH^{3-}	$2.5(2) \times 10^{10}$	3.3	0.4−0.8	80
EGTA	LH^{3-}	7.5×10^{10}	10	0.3	96
1,3-PDTA	LH^{3-}	$6.8(3) \times 10^{10}$	9.1	0.4−0.8	80
HEIDA	L^{2-}	2.0×10^{10}	2.7	0.3	96
NTA	L^{3-}	$<1.5 \times 10^{11}$	<20		79
	LH^{2-}	$4.4(9) \times 10^6$	5.9×10^{-4}		79
$[18]aneO_6$	L	5.92×10^6	7.9×10^{-4}	0.1	97
$Ac_2[18]aneN_2O_4$	LH_2	1.7×10^3	2.3×10^{-7}	0.2	91
	LH^-	2.30×10^8	3.1×10^{-2}	0.2	91
cyclen	LH^+	$8.3(1) \times 10^5$	1.1×10^{-4}	0.2	85
	LH_2^{2+}	1.4(2)	1.9×10^{-10}	0.2	85
DOTA	LH^{3-}	$1.8(4) \times 10^9$	2.4×10^{-1}	0.1	86
	LH_2^{2-}	$7(3) \times 10^3$	9×10^{-7}	0.1	86
DOTAM ($\mathbf{L^4}$)	LH^+	$1.19(4) \times 10^5$	1.6×10^{-5}	0.1	24
$\mathbf{L^1}$	LH^+	$1.36(5) \times 10^6$	1.8×10^{-4}	0.1	this work
$\mathbf{L^2}$	LH^+	$9.8(1) \times 10^6$	1.3×10^{-3}	0.1	this work
$\mathbf{L^3}$	LH^+	$7.8(1) \times 10^6$	1.0×10^{-3}	0.1	this work

[a] EDTA, ethylenediamine-*N*,*N*,*N*′,*N*′-tetraacetate; HEDTA, *N*-(2-hydroxyethyl)ethylenediamine-*N*,*N*′,*N*′-triacetate; EDDDA, ethylenediamine-*N*,*N*′-diacetate-*N*,*N*′-dipropionate; EGTA, 1,2-bis(2-aminoethoxyethane)-*N*,*N*,*N*′,*N*′-tetraacetate; 1,3-PDTA, 1,3-propylenediaminetetraacetate; HEIDA, *N*-(2-hydroxyethyl)iminodiacetate; NTA, nitrilotriacetate; $[18]aneO_6$, 1,4,7,10,13,16-hexaoxacyclooctadecane; $Ac_2[18]aneN_2O_4$, 1,4,10,13-tetraoxa-7,16-diazacyclooctadecane-*N*,*N*′-diacetate; cyclen, 1,4,7,10-tetraazacyclododecane; DOTA, 1,4,7,10-tetraazacyclododecane-*N*,*N*′,*N*″,*N*‴-tetraacetate.

(68) Kasprzyk, S. P.; Wilkins, R. G. *Inorg. Chem.* **1982**, *21*, 3349−3352.
(69) Izatt, R. M.; Bradshaw, J. S.; Nielsen, S. A.; Lamb, J. D.; Christensen, J. J.; Sen, D. *Chem. Rev.* **1985**, *85*, 271−339.
(70) Izatt, R. M.; Pawlak, K.; Bradshaw, J. S.; Bruening, R. L. *Chem. Rev.* **1991**, *91*, 1721−2085.
(71) Izatt, R. M.; Pawlak, K.; Bradshaw, J. S.; Bruening, R. L. *Chem. Rev.* **1995**, *95*, 2529−2586.
(72) Elias, H. *Coord. Chem. Rev.* **1999**, *187*, 37−73.
(73) Eigen, M.; Wilkins, R. G. *Adv. Chem. Ser.* **1965**, *49*, 55−67.
(74) Wilkins, R. G. *Acc. Chem. Res.* **1970**, *3*, 408−416.
(75) Fuoss, R. M. *J. Am. Chem. Soc.* **1958**, *80*, 5059−5061.
(76) Yasunaga, T.; Harada, S. *Bull. Chem. Soc. Jpn.* **1971**, *44*, 848−850.

rate constants (k'_f) that vary between 0.2 and $\sim 6 \times 10^{11}$ M^{-1} s^{-1} and thus fall within the expected range for diffusion-limited rate constants ($10^{10}-10^{11}$ M^{-1} s^{-1}).[77] The favorable electrostatic outer-sphere interactions experienced by the 3-fold negatively charged species tend to hasten the overall formation rates by a factor of 10−100 with respect to water exchange, depending upon the distance of closest approach (*a*) of both partners forming the ion pair. A typical example is provided by $EDTAH^{3-}$ for which $K_{OS} = k'_f/k_{ex} \approx 81$. Solving the Fuoss equation yields an approximate value of 5.1 Å for the parameter *a*. In Table 6 most of the data pertaining to EDTA-type ligands correspond to reaction of aquated lead(II) with the monoprotonated species. Rabenstein and co-workers proposed a stepwise formation of the lead complex that proceeds by dissociation of water molecules followed by bond formation to yield a triscoordinated intermediate in which one end of the partially attached ligand is blocked by the proton residing on the unbound nitrogen atom. Proton transfer to a carboxylate oxygen atom or to a solvent molecule is required before the water substitution proceeds to completion. While proton migration was initially sought to be the rate-limiting step in order to explain the much lower than predicted second-order rate constant found for $NTAH^{2-}$,[78,79] these authors later assumed that it should correspond more likely to formation of one of the first three bonds.[80] Correlating the kinetic data collected for Ni^{2+}, Cu^{2+}, Zn^{2+}, Cd^{2+}, and Pb^{2+}, Margerum suggested an alternate but more probable path in which the proton is shifted from the ammonium to a carboxylate oxygen atom before reaction with the aquated cation.[77] Hence, proton transfer is no longer rate determining, while anchoring to the metal occurs through the protonated carboxylate group. Fuhr and Rabenstein also pointed out that six-membered chelate ring formation was significantly slower compared to five-membered ring closure.[80]

In contrast to open-chain chelates, formation of macrocyclic lead complexes is several orders of magnitude slower. As expected, cryptands with their more rigid polycyclic framework are less reactive.[81,82] All the available data suggest that ion pairing followed by desolvation of the Pb^{2+} cation is not rate limiting.[72,77,83] Indeed, the unfavorable electrostatic interactions expected for $\mathbf{L^1}-\mathbf{L^4}$ cannot solely account for the second-order rate constants appearing in Table 6 that are lower than those predicted by the Eigen−Wilkins theory. Hence, the rate-determining step is taking place after formation of the first metal ion−donor atom bond. Setting the distance of closest approach of both partners forming the ion pair at 5 Å, $K_{OS} = 0.315$ and 0.048 M^{-1} for $\{Pb^{2+}\cdots L\}$ and $\{Pb^{2+}\cdots LH^{+}\}$, respectively. The latter figure is in excellent agreement with the experimental value measured by Palanché et al. for the association of $Fe(OH)_2^{+}$ with the LH_6^{+} form of azotobactin δ.[84] Under these conditions, the product $K_{OS} \times k_{ex}$ is on the order of 2.4×10^9 (L) or 3.6×10^8 M^{-1} s^{-1} (LH^{+}). In comparison, the experimental bimolecular rate constants k_1 and k_3 are about 10 ($\mathbf{L^2}$ and $\mathbf{L^3}$), 250 ($\mathbf{L^1}$), and 3000 times ($\mathbf{L^4}$) lower.

It is well known that attachment of ligating side chains to a cyclic polyamine can dramatically accelerate the complexation reaction.[72] For lead(II) this behavior is best exemplified by comparing the rates, despite the charge difference, reported for $cyclenH^{+}$ ($k'_f = 8.3(1) \times 10^5$ M^{-1} s^{-1})[85] and $DOTAH^{3-}$ ($k'_f = 1.8(4) \times 10^9$ M^{-1} s^{-1}).[86] Of some relevance to the present study, Moreau et al. recently summarized the prolific literature related to the metalation kinetics of $DOTAH_2^{2-}$.[87] Although some mechanistic details still remain a matter of debate, there is general agreement on the rapid formation of an intermediate protonated species in which a lanthanide cation is only bound by the four carboxylate oxygen atoms located above the ring, before slow reorganization leads to inclusion of the metal ion into the macrocyclic cavity. Concerted proton migration from both ammonium sites to bound carboxylate oxygen atoms and concomitant formation of two nitrogen−metal bonds has been envisioned as potential rate-limiting steps affording a second intermediate.[87] In the final step both carboxylic protons are lost, while creation of the last pair of lanthanide−nitrogen bonds requires several weeks.

Accordingly, assistance of the appended amide side chains in the early stage of the Pb^{2+} binding process is also expected for $\mathbf{L^1}-\mathbf{L^3}$, although no kinetic data are available to the best of our knowledge for the incorporation of Pb^{2+} into cyclam. This assumption is also supported by previous observations on neutral cyclam derivatives substituted by 2-hydroxyalkyl groups.[88] However, due to the much lower metal and proton binding affinities of carbamoyl versus carboxylate oxygen atoms, a mechanism similar to that mentioned above for DOTA seems unlikely. While the first two water molecules are certainly displaced by the entering carbonyl oxygen atoms, subsequent interactions with the adjacent tertiary amines bearing both involved arms enable the rapid closing of one and then a second five-membered chelate ring. Rahardjo and Wainwright demonstrated that at least two dangling hydroxyethyl functions are required for accelerating metal insertion into a cyclam framework.[89] Such a sequential arm-by-arm chelation process is also supported by the general

(77) Margerum, D. W.; Cayley, G. R.; Weatherburn, D. C.; Pagenkopf, G. K. *Kinetics and Mechanisms of Complex Formation and Ligand Exchange*; ACS Monograph 174; American Chemical Society: Washington, DC, 1978.

(78) Rabenstein, D. L.; Kula, R. J. *J. Am. Chem. Soc.* **1969**, *91*, 2492−2503.

(79) Rabenstein, D. L. *J. Am. Chem. Soc.* **1971**, *93*, 2869−2874.

(80) Fuhr, B. J.; Rabenstein, D. L. *Inorg. Chem.* **1973**, *12*, 1868−1874.

(81) Cox, B. G.; Garcia-Rosas, J.; Schneider, H. *Nouv. J. Chim.* **1982**, *6*, 397−399.

(82) Cox, B. G.; Garcia-Rosas, J.; Schneider, H.; van Troung, N. *Inorg. Chem.* **1986**, *25*, 1165−1168.

(83) Wilkins, R. G. *Kinetics and Mechanism of Reactions of Transition Metal Complexes*, 2nd ed.; VCH: Weinheim, Germany, 1991.

(84) Palanché, T.; Blanc, S.; Hennard, C.; Abdallah, M. A.; Albrecht-Gary, A. M. *Inorg. Chem.* **2004**, *43*, 1137−1152.

(85) Kodama, M.; Kimura, E. *J. Chem. Soc., Dalton Trans.* **1977**, 2269−2276.

(86) Pippin, C. G.; McMurry, T. J.; Brechbiel, M. W.; McDonald, M.; Lambrecht, R.; Milenic, D.; Roselli, M.; Colcher, D.; Gansow, O. A. *Inorg. Chim. Acta* **1995**, *239*, 43−51.

(87) Moreau, J.; Guillon, E.; Pierrard, J. C.; Rimbault, J.; Port, M.; Aplincourt, M. *Chem.—Eur. J.* **2004**, *10*, 5218−5232.

(88) Dey, B.; Coates, J. H.; Duckworth, P. A.; Lincoln, S. F.; Wainwright, K. P. *Inorg. Chim. Acta* **1993**, *214*, 77−84.

(89) Rahardjo, S. B.; Wainwright, K. P. *Inorg. Chim. Acta* **1997**, *255*, 29−34.

Scheme 2

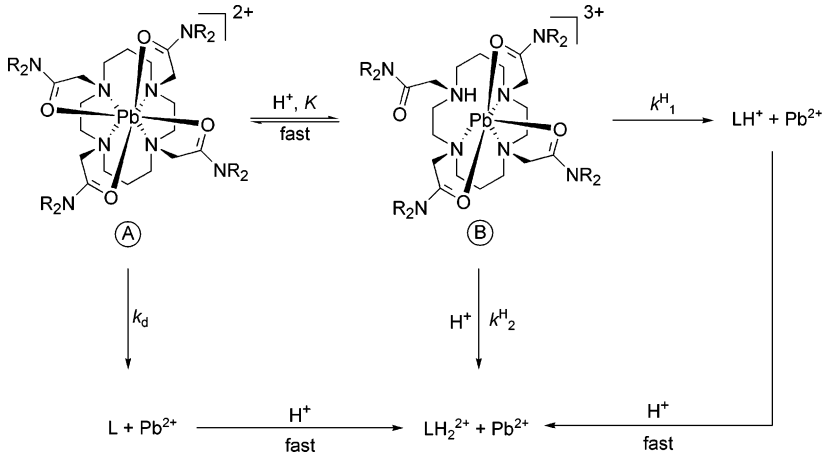

formation mechanism of metal−peptide complexes.[90] Once the cation has been brought in the vicinity of the cyclam ring, the fifth bond formation could involve a nitrogen atom located on the opposite side of the already bound amide arms. Deprotonation of the ammonium group and binding of the appended amide substituent is supposed to occur in the last stages, leading to the final octacoordinated complex. In all likelihood, one of those late steps should then be rate determining.

Dissociation Kinetics. The proton-concentration dependence exhibited by the pseudo-first-order rate constants k_{obs} displayed in Figure 7 clearly illustrates the increasing lability of the complexes in the order $Pb(\mathbf{L^3})^{2+} < Pb(\mathbf{L^2})^{2+} \ll Pb(\mathbf{L^1})^{2+}$, which corresponds to the reverse sequence of the thermodynamic β_{110} stability constants (Table 2). Moreover, the observed rate law (eq 15) suggests a complex reaction scheme with multiple dissociation paths involving rapid formation of a protonated intermediate. The experimental data support the mechanism depicted in Scheme 2.

According to the kinetic parameters collected in Table 5, the less efficient pathway corresponds to the spontaneous self-dissociation (k_d) of the octacoordinated $Pb(L)^{2+}$ complexes labeled A in Scheme 2, followed by the fast protonation of the liberated ligand. The associated first-order rate constants k_d primarily reflect the inertia of the complexes in the absence of protons (solvent-assisted dissociation). As expected, the k_d value was the highest for the less stable $Pb(\mathbf{L^1})^{2+}$ species ($k_d = 9(4)\ s^{-1}$), while it became statistically insignificant in the case of $Pb(\mathbf{L^3})^{2+}$.

The second demetalation route assumes the fast protonation of complex A which is in equilibrium (K) with a monoprotonated intermediate B. Since amines are much stronger bases than amidic oxygen atoms, it is assumed that the entering proton first breaks one metal−nitrogen bond, giving rise to an ammonium site.[60] It is anticipated that the protonated nitrogen atom will move away from the coordination center as much as possible due to charge repulsion, inducing the complete dechelation of the aminocarbamoyl arm for steric reasons. Intermediate B is therefore assimilated to a hexacoordinated Pb^{2+} species. The subsequent dissociation of the remaining donor atoms is controlled by the first-order rate constant k^H_1. The value of the preequilibrium constant K is sensitive to the electronic features (σ-donation) of the macrocycle, although there is no direct proportionality between the complex and the free ligand protonation constants. In contrast, the first-order rate constants k^H_1 associated with dissociation of intermediate B does not depend on the nature of the ligand.

Alternatively, complex B can also dissociate according to a bimolecular reaction with a second proton (k^H_2), directly releasing a Pb^{2+} ion and one molecule of diprotonated ligand LH_2^{2+}. This latter pathway becomes operative for total acid concentrations above ca. 0.01 M and predominates at concentrations higher than 0.02 M. The kinetic data in Table 5 show a regular decrease of the second-order rate constant k^H_2 as the steric bulk of the *N*-terminal amide substituents increases. Accordingly, $Pb(\mathbf{L^1}H)^{3+}$ dissociates about 1.5 times faster than $Pb(\mathbf{L^2}H)^{3+}$ or $Pb(\mathbf{L^3}H)^{3+}$, confirming the protective role exerted by the alkyl groups against the proton attack.

In related work the same rate law and mechanism were deduced for the acid-promoted dissociation of a pentacoordinated 1,4,8,11-tetraazacyclotetradecane-1,8-bis(methylphosphonato)copper(II) complex by Kotek et al.[60] and of the lead complex formed with 1,4,7,10-tetraoxa-7,16-diazacyclooctadecane-*N*,*N*′-diacetic acid by Laing et al.[91] The latter authors reported similar kinetic parameters to those found herein ($K = 100(40)\ M^{-1}$, $k^H_1 = 18(11)\ s^{-1}$, and $k^H_2 = 9(4)\ M^{-1}\ s^{-1}$; $T = 298$ K; $I = 0.2$ (Li,H)ClO_4). In contrast, the lifetime of $Pb(DOTA)^{2-}$ ($k_{obs} = 6.15 \times 10^{-5}\ s^{-1}$)[86] is much longer in acidic conditions ($[H^+] = 0.02$ M; $I = 0.1$ M; $T = 298$ K) than those measured for the cyclam-based tetraamides ($k_{obs} = 277\ s^{-1}$ for $Pb(\mathbf{L^1})^{2+}$). This difference highlights the extraordinary inertness generally observed for all metal complexes incorporating a cyclen unit appended with acetate groups.[92−94] Moreover, the presence of additional protonation

(90) *Metal Ions in Biological Systems. Concepts on Metal Ion Toxicity*; Sigel, H., Ed.; Marcel Dekker: New York, 1986; Vol. 20.

(91) Laing, J. L.; Taylor, R. W.; Chang, C. A. *J. Chem. Soc., Dalton Trans.* **1997**, 1195−1200.

(92) Toth, E.; Brücher, E.; Lazar, I.; Toth, I. *Inorg. Chem.* **1994**, *33*, 4070−4076.

(93) Wang, X.; Jin, T.; Comblin, V.; Lopez-Mut, A.; Merciny, E.; Desreux, J. F. *Inorg. Chem.* **1992**, *31*, 1095−1099.

sites also has some important consequences from a mechanistic point of view. As shown by Pippin et al.,[86] formation of the Pb(DOTAH) intermediate ($K = 2.0(5) \times 10^3$ M^{-1}) most probably involves the initial protonation of a carboxylate oxygen atom. The proton then transfers to an amine ($K = 5.1(5)$ M^{-1}) before a second proton is rapidly taken up. The rate-limiting step has been assigned to dissociation of the neutral $Pb(DOTAH_2)$ complex, which is characterized by a first-order rate constant of $6.7(3) \times 10^{-4}$ s^{-1}. Since amide groups are much more acidic than carboxylates, it is anticipated that $Pb(\mathbf{L^4})^{2+}$ would be even more inert,[24] this assumption being supported by the fact that this complex keeps its integrity in 0.5 M HCl as stressed by Maumela et al.,[95] whereas $Pb(DOTA)^{2-}$ is fully decomposed at pH values below 2.

Conclusion

A combination of potentiometric and absorption spectroscopic data allowed us to characterize the formation and the dissociation mechanism of octacoordinated lead complexes of primary and tertiary tetrakiscarbamoylmethyl cyclam derivatives. In solution, the Pb^{2+} cation is entrapped in a molecular cage constituted by the four macrocyclic nitrogen and the four amidic oxygen atoms. The weaker proton and lead binding constant found for $\mathbf{L^1}$ in comparison to $\mathbf{L^2}$ and $\mathbf{L^3}$ can be explained by the existence in solution of hydrogen bonds between each lone pair of electrons belonging to an amine and one terminal NH_2 hydrogen atom of the appended substituent, as found in the crystal structure for the free-base macrocycle $\mathbf{L^1}$. However, changes in the lead complex stabilities and ligand basicities are integrally compensated, so that all three macrocycles exhibit a similar uptake capacity for identical proton, metal, and ligand concentrations. The complexation reaction proceeds according to an Eigen−Winkler mechanism with a single, albeit late, rate-determining step. The two first bond formations likely involve an oxygen atom from two amide groups, which are immediately followed by chelate ring closure through nitrogen−lead interactions. The lower intrinsic reactivity of the acetamide ligand $\mathbf{L^1}H^+$ compared to the tertiary amides $\mathbf{L^2}H^+$ and $\mathbf{L^3}H^+$ is easily understood by considering that intramolecular hydrogen bonds are preserved in the monoprotonated state. However, due to the lower basicity of $\mathbf{L^1}$, the apparent pseudo-first-order complexation rate constants are about 10 times higher than those measured for $\mathbf{L^2}$ and $\mathbf{L^3}$ in the investigated p[H] range 4−7. Finally, the proton-mediated dissociation studies of the complexes evidenced a fast release of the lead cation in a single rate-limiting step. The observed rate law supports a demetalation mechanism with three parallel pathways. Besides spontaneous self-decomplexation of the reagent, the kinetics is controlled in weakly acidic conditions by the first-order dissociation of a rapidly formed monoprotonated intermediate and at higher acid concentrations by the bimolecular attack of a second scavenging proton.

Acknowledgment. This paper is dedicated to Dr. Anne-Marie Albrecht-Gary on the occasion of her birthday. The work was carried out within the framework of the French governmental project "Réduire la teneur du plomb dans l'eau" (contract no. 99V0367−Ministère Délégué à la Recherche et aux Nouvelles Technologies and Ministère de l'Equipement, des Transports et du Logement) and also supported by the Centre National de la Recherche Scientifique (CNRS) and the Conseil Régional de Bourgogne. F.C. thanks the Ministère Délégué à la Recherche et aux Nouvelles Technologies for a Ph.D. scholarship. We also acknowledge A. Bucaille for providing some compounds.

Supporting Information Available: $^1H-^1H$ NMR COSY spectrum of $[Pb(\mathbf{L^2})](ClO_4)_2$ in DMSO-d_6, tables of the pseudo-first-order rate constants (k_{obs}) for the formation and proton-assisted dissociation of $Pb(\mathbf{L^1})^{2+}$, $Pb(\mathbf{L^2})^{2+}$, and $Pb(\mathbf{L^3})^{2+}$, and X-ray crystallographic files in CIF format for the structure determinations. This material is available free of charge via the Internet at http://pubs.acs.org.

IC0508019

(94) Caravan, P.; Ellison, J. J.; McMurry, T. J.; Lauffer, R. B. *Chem. Rev.* **1999**, *99*, 2293−2352.
(95) Maumela, H.; Hancock, R. D.; Carlton, L.; Reibenspies, J. H.; Wainwright, K. P. *J. Am. Chem. Soc.* **1995**, *117*, 6698−6707.
(96) Kodama, M.; Namekawa, K.; Horiuchi, T. *Bull. Chem. Soc. Jpn.* **1974**, *47*, 2011−2016.
(97) Geary, C. D.; Weber, S. G. *Anal. Chem.* **2003**, *75*, 6560−6565.